AD-A076 578　　NAVAL POSTGRADUATE SCHOOL　MONTEREY CA　　　　　　　　　　　F/G 13/2
MEASUREMENTS OF JET DISPERSIONS SIMULATED IN AN AERONAUTICAL WI--ETC(U)
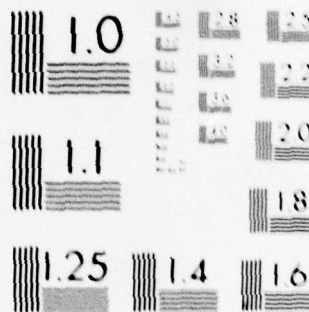SEP 79　J V BRENDMOEN

UNCLASSIFIED　　　　　　　　　　　　　　　　　　　　　　　　　　　　　　　　NL

/ OF /

AD
A076578

END
DATE
FILMED
12-79
DDC

MICROCOPY RESOLUTION TEST CHART
NATIONAL BUREAU OF STANDARDS-1963-A

NAVAL POSTGRADUATE SCHOOL
Monterey, California

Masters **THESIS**

Measurements of Jet Dispersions Simulated
in an Aeronautical Wind Tunnel,

by

Jack Vernon Brendmoen

Sep   1979   94

Thesis Advisor   D. W. Netzer

Approved for public release; distribution unlimited

251 450

79 14 11 040

REPORT DOCUMENTATION PAGE		READ INSTRUCTIONS BEFORE COMPLETING FORM
1. REPORT NUMBER	2. GOVT ACCESSION NO.	3. RECIPIENT'S CATALOG NUMBER
4. TITLE (and Subtitle) Measurements of Jet Dispersions Simulated in an Aeronautical Wind Tunnel		5. TYPE OF REPORT & PERIOD COVERED Master's Thesis; September 1979
		6. PERFORMING ORG. REPORT NUMBER
7. AUTHOR(s) Jack Vernon Brendmoen		8. CONTRACT OR GRANT NUMBER(s) N6237679WR00014
9. PERFORMING ORGANIZATION NAME AND ADDRESS Naval Postgraduate School MMonterey, California 93940		10. PROGRAM ELEMENT, PROJECT, TASK AREA & WORK UNIT NUMBERS
11. CONTROLLING OFFICE NAME AND ADDRESS Naval Air Propulsion Center Trenton, New Jersey 08628		12. REPORT DATE September 1979
		13. NUMBER OF PAGES 93
14. MONITORING AGENCY NAME & ADDRESS(if different from Controlling Office) Naval Postgraduate School Monterey, California 93940		15. SECURITY CLASS. (of this report) Unclassified
		15a. DECLASSIFICATION/DOWNGRADING SCHEDULE

16. DISTRIBUTION STATEMENT (of this Report)

Approved for public release; distribution unlimited

17. DISTRIBUTION STATEMENT (of the abstract entered in Block 20, if different from Report)

18. SUPPLEMENTARY NOTES

19. KEY WORDS (Continue on reverse side if necessary and identify by block number)

Air Pollution
Jet Dispersion
Navy

20. ABSTRACT (Continue on reverse side if necessary and identify by block number)

A neutrally stable atmospheric surface layer was suitably simulated in a low speed wind tunnel by tripping the boundary layer with a fence and letting the turbulent flow develop over a length of roughness elements. Jet exhaust dispersion characteristics, simulated by a burner/nozzle system, were investigated by measuring the horizontal and vertical temperature profiles at axial stations downwind from the nozzle exit. Dispersion sensitivity to different

DD FORM 1473 EDITION OF 1 NOV 65 IS OBSOLETE
1 JAN 73
(Page 1)   S/N 0102-014-6601 |

nozzle exit conditions, angles of incidence to the wind, and nozzle surface blockage were investigated. The results were compared to dispersion methods used in the Air Quality Assessment Model (AQAM). It was found that the experimental jet penetration length was much shorter than that assumed by AQAM, and that a plume rise existed, which is not included in the current AQAM model. Required inputs of the initial dispersion coefficients were determined as a function of wind direction.

Accession For

NTIS GRA&I

DDC TAB

Unannounced

Justification

By

Distribution/

Availability Codes

Dist | Avail and/or special

A

Measurements of Jet Dispersions
Simulated in an
Aeronautical
Wind Tunnel

by

Jack Vernon Brendmoen
Lieutenant, United States Navy
B.S.M.E., University of Nebraska 1973

Submitted in partial fulfillment of the
requirements for the degree of

MASTER OF SCIENCE IN AERONAUTICAL ENGINEERING

from the
NAVAL POST GRADUATE SCHOOL
September 1979

Author: _____

Approved by: _____
                                          Thesis Advisor

_____
Chairman, Department of Aeronautics

_____
Dean of Sciences and Engineering

3

ABSTRACT

A neutrally stable atmospheric surface layer was
suitably simulated in a low speed wind tunnel by tripping
the boundary layer with a fence and letting the turbulent
flow develop over a length of roughness elements. Jet
exhaust dispersion characteristics, simulated by a
burner/nozzle system, were investigated by measuring the
horizontal and vertical temperature profiles at axial
stations downwind from the nozzle exit. Dispersion
sensitivity to different nozzle exit conditions, angles of
incidence to the wind, and nozzle surface blockage were
investigated. The results were compared to dispersion
methods used in the Air Quality Assessment Model (AQAM). It
was found that the experimental jet penetration length was
much shorter than that assumed in AQAM, and that a plume
rise existed, which is not included in the current AQAM
model. Required inputs of the initial dispersion
coefficients were determined as a function of wind
direction.

4

TABLE OF CONTENTS

LIST OF TABLES

LIST OF FIGURES

TABLE OF SYMBOLS

JD	Jet Diameter
p	Pressure
T_σ	Temperature at One Standard Deviation from the Mean
u	Average Velocity Component in the x Direction
u´	Fluctuating Velocity Component in the x Direction
u.	Wall Friction Velocity
U_∞	Free Stream Velocity in the Wind Tunnel
w	Average Velocity Component in the z Direction/ Jet Plume Lateral Dimension
w´	Fluctuating Velocity Component in the z Direction
x	Axial Direction
y	Lateral Direction
z	Vertical Direction
z_0	Roughness Length
Δz	Jet Plume Vertical Dimension
κ	Von Karman's Constant
ν	Kinematic Viscosity
ρ	Density
$\overline{\rho u' w'}$	Turbulent Shear Stress
σ	Standard Deviation
σ_{y_0}	Initial Dispersion Coefficient in the Lateral Direction
σ_{z_0}	Initial Dispersion Coefficient in the Vertical Direction

σ_y Dispersion Coefficient for the
Lateral Direction

σ_z Dispersion Coefficient for the
Vertical Direction

τ_o Wall Shear Stress

τ Shear Stress

ACKNOWLEDGEMENTS

I.   INTRODUCTION

The Air Force has developed an Air Quality Assessment
Model (AQAM) to predict the dispersion of pollutants emitted
from typical Air Base related sources (Ref. 1, 2 and 3).
That model has also been modified to better simulate
operations from a Naval Air Station (Ref. 4 and 5). The
full model consists of three computer programs: Source
Inventory, Short Term and Long Term Dispersion. In the
Short Term Model hourly averaged concentrations are
predicted over a grid of receptors. Air-base, aircraft, and
off air-base (environ) sources are considered and are
modeled as point, area, or line sources as appropriate.

In the Short Term Model, the jet exhausts from aircraft
during taxi and takeoff are treated as line sources with no
plume rise. Initial plume dimensions must be estimated as
well as the distance the jet "penetrates" the atmosphere
before coming essentially to rest relative to the ambient
wind. Stationary sources such as engine run up test stands
and test cells are treated as points sources. Likewise, the
initial plume dimensions must be estimated and a
determination whether plume rise is a factor must be made.
The model then uses these input data to determine an initial
dispersion coefficient from which a pseudo upwind point or

line source is located. The sigma's, or dispersion
coefficients, are based on the stability class of the
atmosphere and the downwind distance or travel time for an
elevated, relatively low velocity source. There is a
question then, as to the applicability of these dispersion
coefficients to turbojet exhausts which are often sonic,
have high shear stress/turbulent mixing characteristics and
have different turbulence scales than typical exhaust
stacks. Evidence that there is a discrepancy has been
indicated by an Air Force study (Ref. 6) which presented a
pictorial investigation of the effects of atmospheric
stability on a jet exhaust. It is evident that qualitative
and quantitative data are needed to characterize the
dispersion of a turbojet exhaust during ground operations.
This investigation attempted to determine turbojet exhaust
dispersion as a function of jet characteristics and wind
direction under laboratory simulated, neutrally stable
atmospheric conditions.

The first part of the study involved the correct
simulation of the lower portion of the atmosphere in an
aeronautical type wind tunnel. Published studies (Refs. 7,
8 and 9) have indicated that it is not sufficient to
simulate only the mean velocity profile of the atmosphere.
The turbulent structure of the atmosphere must also be
correctly modeled simultaneously with the mean velocity

profile. Proper simulation can be accomplished following
the work of Sundaram and Ludwig (Ref. 7), tripping the
boundary layer with a suitable fence at the entrance of the
wind tunnel test section and then letting the turbulent flow
develop over a length of roughness elements. Suitable
matching between the boundary layer trip and the roughness
elements then results in an area of constant shear stress
which adequately models the atmospheric flow.

Once an atmospheric surface layer has been suitably
simulated, a turbojet exhaust must then be simulated. If it
is assumed that heat and mass have the same turbulent
diffusion characteristics, then the dispersion rates of
pollutants can be determined by measuring the temperature
distributions in the vertical and horizontal directions.

In this investigation data were obtained for varying
angles of incidence to the oncoming wind for choked and
unchoked nozzle flow conditions, for two jet temperatures,
and for two conditions of nozzle surface blockage. The data
were compared to the dispersion routines used in the AQAM
computer program.

II.   ATMOSPHERIC SIMULATION

In order to make meaningful wind tunnel measurements to
determine jet aircraft exhaust dispersion rates during taxi,
idle and takeoff modes of operation it was necessary to
correctly model the lower structure of the atmosphere.
Sundaram and Ludwig (kef. 7) have published a theoretical
study of the requirements for the modeled flow and an
experimental study of the flow generated by wind tunnel
techniques. This reference was used as the principal guide
in modeling the atmospheric surface layer in a wind tunnel
at the Naval Postgraduate school. Supplementary discussions
are presented in Refs. 10-12

A.   THEORETICAL REQUIREMENTS FOR ATMOSPHERIC MODELING

Reference 13 describes the atmospheric boundary layer as
a turbulent layer which is influenced by a combination of
actions due to surface friction, thermal stratification, and
Coriolis force. The atmospheric boundary layer is divided
into two distinct layers. The lower region called the
surface boundary layer extends up to a nominal height of 100
meters. The region above the surface layer is called the
Ekman layer and extends up to a height of about 1000 meters.
In the Ekman layer the wind direction changes with height so

17

that an equilibrium balance is maintained between the Coriolis, pressure, and shear forces. In the surface layer, however, the wind direction is generally considered to remain constant, the Coriolis force is not an important parameter and, therefore, the variations in shear stress and vertical momentum with increasing height are considered to be negligible. The Monin-Obukhov theory, Ref.14, and other surface layer theories make the assumption that the flow characteristics close to the ground can be expressed entirely in terms of conditions at the surface. This assumption means that the conditions close to the surface are independent of the conditions in the Ekman layer. The boundary layer equation for a flat plate with no pressure gradient is

$$u\partial u/\partial x + w\partial u/\partial z = \partial\tau/\partial z. \qquad (1)$$

Near the surface, the left hand side of equation (1) will be small. The shear stress can, therefore, be considered to be independent of height in the region close to the surface. This assumption is important because a simple theoretical description of a neutrally stable atmospheric boundary layer is made possible which permits the simulation of such a flow in an experimental wind tunnel. A turbulent, neutrally

18

stable flow structure in the atmospheric surface boundary
layer can be described entirely by the following parameters;
the kinematic viscosity ν, the friction velocity u_*, and
the roughness parameter z_0 (Ref. 7). u_* is defined as being
equal to $(\tau_0/\rho)^{1/2}$ and z_0 is a length scale which describes
the influence of a rough surface on a particular flow. Most
atmospheric boundary layers are observed to have no laminar
sublayer near the surface and are described to be fully
aerodynamically rough. Using the above parameters, an
aerodynamically rough flow exists if (Ref. 7)

$$z_0 u_* / \nu > 3. \tag{2}$$

If z_0 is $\ll$ than the vertical dimension of the boundary
layer, then the mean velocity profile of the wind is given
in logrithmic form by the relationship (Ref. 7)

$$u/u_* = (1/\kappa) \ln (z/z_0) \, , \tag{3}$$

where u is the average velocity, z is the vertical distance
from the surface and κ is Von Karman's constant. This
equation is a form of the well known law of the wall and is

19

indicative of the interaction between the air flow above a
given surface and that surface. The existence of such a
velocity profile implies (Ref. 7) that the flow is
horizontally homogeneous. By neglecting the Coriolis force,
a neutrally stable, horizontally homogeneous flow obeys the
following relationship (Ref. 7)

$$\partial\tau/\partial z = (-1/\rho) \; \partial p/\partial x \qquad\qquad (4)$$

which describes the vertical variation of shear stress with
the horizontal pressure gradient. If constant shear stress
is a requirement for a neutrally stable atmosphere, then
equations (2) through (4) identify additional requirements
for a such a flow. The additional requirements are; a fully
aerodynamically rough flow, horizontal homogeneity, and the
absence of a pressure gradient. To accurately model the
atmosphere these requirements must be strictly adhered to.
If these requirements are strictly maintained in a
laboratory flow, then it can be expected that the flow will
be similar to the atmospheric surface layer. Strict
horizontal homogeneity, however, is extremely difficult to
obtain in the laboratory. Partial simulation, therefore,
generally has to be imposed. A complete discription of the
effects of partial simulation is given in reference 7 and

will not be repeated here. The conclusion reached from reference 7 regarding partial simulation was that a laboratory flow which was fully aerodynamically rough, nearly horizontally homogeneous and relatively free from pressure gradients was a reasonable model for a neutrally stable atmosphere. The generation of such a flow is described in the next section of this report.

B. EXPERIMENTAL REQUIREMENTS TO SIMULATE ATMOSPHERIC FLOWS

In the previous section the requirements for simulating neutrally stable atmospheric flows were discussed. That is; to correctly model the flow, it must be fully aerodynamically rough, horizontally homogeneous, free of pressure gradients and the shear stress must be constant in the vertical direction. Aircraft jet exhaust dispersion in the "near ground" environment was the primary concern of this investigation; therefore only the surface layer of the atmosphere was modeled. As discussed previously, this was possible since both the atmospheric flow and the experimental flow are described completely in terms of conditions at the surface (ie. the parameters u_*, z_0, and ν). The similarity requirements were, therefore, not a function of the geostrophic wind in the real flow nor a

21

function of the free stream velocity in the modeled flow.
Horizontal homogeneity cannot be strictly satisfied since
for an experimental flow over a flat plate, equilibrium
conditions change continually as a function of downstream
distance (Ref. 7). It was not sufficient, therefore, to
simply compare the mean velocity profile of an atmospheric
flow with that of a simulated flow at one location within
the wind tunnel. The additional measurements which were
required for partial simulation are described in reference
7. Since the atmosphere is assumed to exhibit a logarithmic
mean velocity profile, this part of the similarity
requirement can be easily verified. In reference 7 the
turbulence intensity and the integral scale of turbulence
were also measured and compared to available atmospheric
data. The turbulence intensity measurements in this
experiment were compared to the results of reference 7.
Integral scales of turbulence were not measured. For
virtually identical experimental set-ups it was assumed that
if all other experimental measurements compared favorable to
those of reference 7, then the scales of turbulence would
also compare favorably.

C. EXPERIMENTAL APPARATUS AND MEASUREMENTS

1. Wind Tunnel Modifications

The experiment was conducted in a low speed wind
tunnel at the Naval Postgraduate School (NPS), Monterey, Ca.
The wind tunnel draws ambient air from the surrounding area
into a 5 X 5 foot test section approximately 21 feet long.
In order to be comparable with the wind tunnel used in
reference 7, the wind tunnel at the Naval Postgraduate
School was modified in the following manner. A false
ceiling was installed to maintain an approximate zero
pressure gradient in the axial direction. A two inch high
boundary layer trip constructed of wood was placed across
the entrance to the test section. The trip was followed by
2.5 X 2.5 feet square sections of roughness elements which
covered the entire floor of the test section. The roughness
elements were 4 sided regular pyramids which were 0.75
inches square at the base and 0.75 inches in height. They
were constructed out of 1.5 inch thick fiberboard. The
tunnel and roughness elements are shown in figure 1.

2. Pressure Measurements

Six, 1/8 inch diameter pressure taps spaced 4 feet
apart, were mounted flush along the centerline of the wind

tunnel wall. The differential area required to maintain a zero pressure gradient in the axial direction was determined from an initial set of pressure readings. The false ceiling which implemented the required area change was then installed and the pressure readings were again taken to verify the required zero axial pressure variation.

3. Electronic Equipement

All velocity related measurements were taken with a Thermo Systems Inc. linearized hotwire anemometer system. DISA single wire and cross wire probes and probe holders were used with the anemometer system (fig. 2 and 3). A DC digital voltmeter and a true RMS meter were used to record the steady and fluctuating single wire probe data respectfully. A model 1015C Thermo Systems Inc. correlator was used in conjunction with the cross wire outputs to obtain the sum and difference of the two signals (fig. 4). The true RMS meter was also used to record the cross wire outputs via the correlator. The hotwire probes were mounted under the wind tunnel such that the probes traversed the wind tunnel in a vertical direction. A Spectral Dynamics, Spectra-Scope Model SD-330 frequency counter was used in conjunction with the measurement of the centerline velocity (fig. 5).

4.   Wind Tunnel Centerline Velocity Measurements

The maximum velocity expected in the wind tunnel was between 40 and 50 feet per second. Existing pitot-static systems at NPS were not sensitive to this small velocity. Therefore, the relationship between the Strouhal Number and the Reynolds Number was used to determine the centerline velocity (Ref. 15). The Strouhal number relates the velocity of a flow to the frequency at which vortices are shed behind a circular cylinder which is immersed in that flow.

Sn(Strouhal Number) = (freq. X diam. of cyl.) / velocity.

A 0.075 inch diameter stainless steel wire was attached to a collar which was fitted over a single hotwire probe such that the hotwire was in only one wake (shed vortex sheet) of the cylinder (fig. 6). The probe, collar and hotwire combination was placed perpendicular to flow at the centerline of the tunnel. With the tunnel on, the hotwire system was sensitive to the velocity of the free stream and the output was observed and recorded on the frequency counter.   The observed frequency of shed vorticies and the unique relationship between the Strouhal Number and the Reynolds Number were used to iteratively determine the

25

velocity of the free stream.

5. Velocity Profile Measurements

The mean velocity profile measurements were made
using the single hotwire apparatus.   The hotwire system was
calibrated in the linear mode such that the centerline
velocity was made equal to one volt. The single wire was
also calibrated for flow direction sensitivity. This was
accomplished by rotating the probe umtil a maximun reading
was observed on the DC digital voltmeter. It was then
assumed that the probe was perpendicular to the flow. All
subsequent measurements were referenced to this direction.
The linearized output was averaged through a ten second time
constant before being displayed on the DC digital voltmeter.
The velocity profile was obtained by recording the DC value
of the hotwire output as it traversed the wind tunnel in the
vertical direction. Vertical measurements were referenced
to the top of the roughness elements and were measured to
within an accuracy of 0.020 inches with respect to that
reference. Velocity profiles were obtained at two axial
locations. The locations were 72 inches and 109 inches
downwind from the boundary layer trip at the entrance to the
test section. The two axial measurements were necessary to
ensure the required degree of uniformity in the jet
dispersion region.

26

6. Turbulence/Shear Stress Measurements

The cross wire system described earlier was used to
measure the turblence intensities and shear stresses
directly. The cross wire was calibrated such that the
linearized output for each wire was of equal sensitivity.
This was accomplished by first orienting one wire normal to
the flow and then adjusting its sensitivity to the proper
level. The probe was then re-oriented so that the second
wire was normal to the flow and its sensitivity was then
matched to that of the first wire. For data acquisition,
the probe was oriented axially such that the longitudinal
turbulence intensity was proportional to the RMS value of
the sum of the cross wire outputs. Likewise, for the same
orientation, the vertical turbulence intensity was
proportional to the RMS value of the difference of the cross
wire outputs. The turbulent shear stress is defined as
$- \rho \overline{u'w'}$. This shear stress was obtained directly since $\overline{u'w'}$
is proportional to the square of the sum minus the square of
the difference of the cross wire outputs. Like the single
wire data, the cross wire data was recorded as the probe was
traversed in the vertical direction at the same two axial
locations. For redundancy, the vertical profile of
turbulence intensity was also measured using the single wire
probe.

D. RESULTS AND DISCUSSION

All the measurements obtained at the two axial
locations, ie. 72 and 109 inches from the entrance of the
wind tunnel test section, were taken with a wind tunnel
center line velocity of approximately 40 feet per second.

1. u_* and z_0

From the law of the wall,

$$u/u_* = 5.75 \log z/z_0 \qquad (5)$$

Equation (5) can be rewriten as

$$u/U_\infty = (u_* /U_\infty) 5.75 (\log z - \log z_0). \qquad (6)$$

When u /U_∞ is plotted vs. $\log z$,

$$slope = 5.75 (u_* /U_\infty). \qquad (7)$$

u/U$_\infty$ vs. log z was plotted for both axial positions and a
least squares fit was obtained through the data points
(figures 7 and 8). The slopes were measured and u$_*$ was
determined by;

$$u_* = (\text{slope} \cdot U_\infty)/5.75. \tag{8}$$

u$_*$ values of 2.32 and 2.52 feet per second were obtained at
the 72 and 109 inch positions repectively. Using the least
squares fit data, the calculated u$_*$ was used to determine z$_0$
by;

$$\log z_0 = \log z - u/(5.75 \cdot u_*) \tag{9}$$

z$_0$ values of 0.0215 and 0.0326 were obtained at 72 and 109
inches respectively.

2. <u>Vertical Distribution of Shear Stress</u>

Since u$_*$ is proportional to the shear stress,

$$u_* = \sqrt{\tau_0/\rho} = \sqrt{-\rho\overline{u'w'}/\rho} = \sqrt{\overline{u'w'}} \tag{10}$$

a measure of the average shear stress for each radial
position can be obtained from the mean velocity profile
data. Non-dimensionalizing by $U\infty^2$;

$$\overline{u'w'} / U\infty^2 = (u_* /U\infty)^2 \qquad (11)$$

The measured shear stress, $\overline{u'w'}$, from the cross wire data,
was also non-dimentionalized by $U\infty^2$ and plotted as a
function of the vertical distance above the roughness
elements for both axial positions. Figure 9 presents the
cross-wire data. Also shown are the values of average
stress determined from the law of the wall.

Figures 10 and 11 compare the results with those
presented in reference 7. It is observed that the shear
stress continued to increase until very near the wall
whereas the shear stress from reference 7 began to decay
further from the wall. Figure 10 shows that the shear
stress was approximately constant for heights from 2 to 5
inches above the roughness elements at the 72 inch position.
At the 109 inch position (fig. 11), the shear stress decayed
gradually from the near wall region. In an attempt to

modify the near wall shear stress distribution, different
combinations of trip heights and wind speeds were tried.
This proved to be unsuccessful. The mean velocity profile
was observed to vary much more rapidly in the axial
direction and the relatively constant shear stress region
obtained with the two inch trip was destroyed in varying
degrees depending on which trip or what tunnel speed was
used. There was also a somewhat greater variation in
horizontal homogeneity in this experiment relative to
reference 7. This was reflected in the increased slope of
figure 8 over that of figure 7. This was also reflected in
figure 9 by noting that the average shear stress differed by
about 20 percent between the two positions. Moreover, z_0
increased by about 50 percent over the axial range compared
to about 30 percent for the experiment of reference 7. It
was also noted in reference 7, however, that the degree of
uncertainty in the atmosphere may be much larger than the 30
percent figure.

3. Vertical and Horizontal Turbulence Intensities

Figures 12 and 13 compare the measured vertical and
horizontal turbulence intensity measurements at the two
axial locations with the data of reference 7. In general,
the vertical and horizontal data agreed extremely well with
the data of reference 7. The horizontal turbulence was a

31

little lower for both positions in the range of z/z_0 from 1 to 30 or 40. This corressponded to a height of about one inch above the roughness elements and was the area of difference noted in figures 10 and 11.

Since, (1) a region of constant shear stress was obtained in good agreement with reference 7, (2) the turbulence intensities were relatively constant over the same region, (3) the roughness parameter z_0 was comparable to that of reference 7, and (4) equation (2) was satisfied, the simulated atmospheric surface layer was considered to be adequate for the initial study of jet exhaust dispersion.
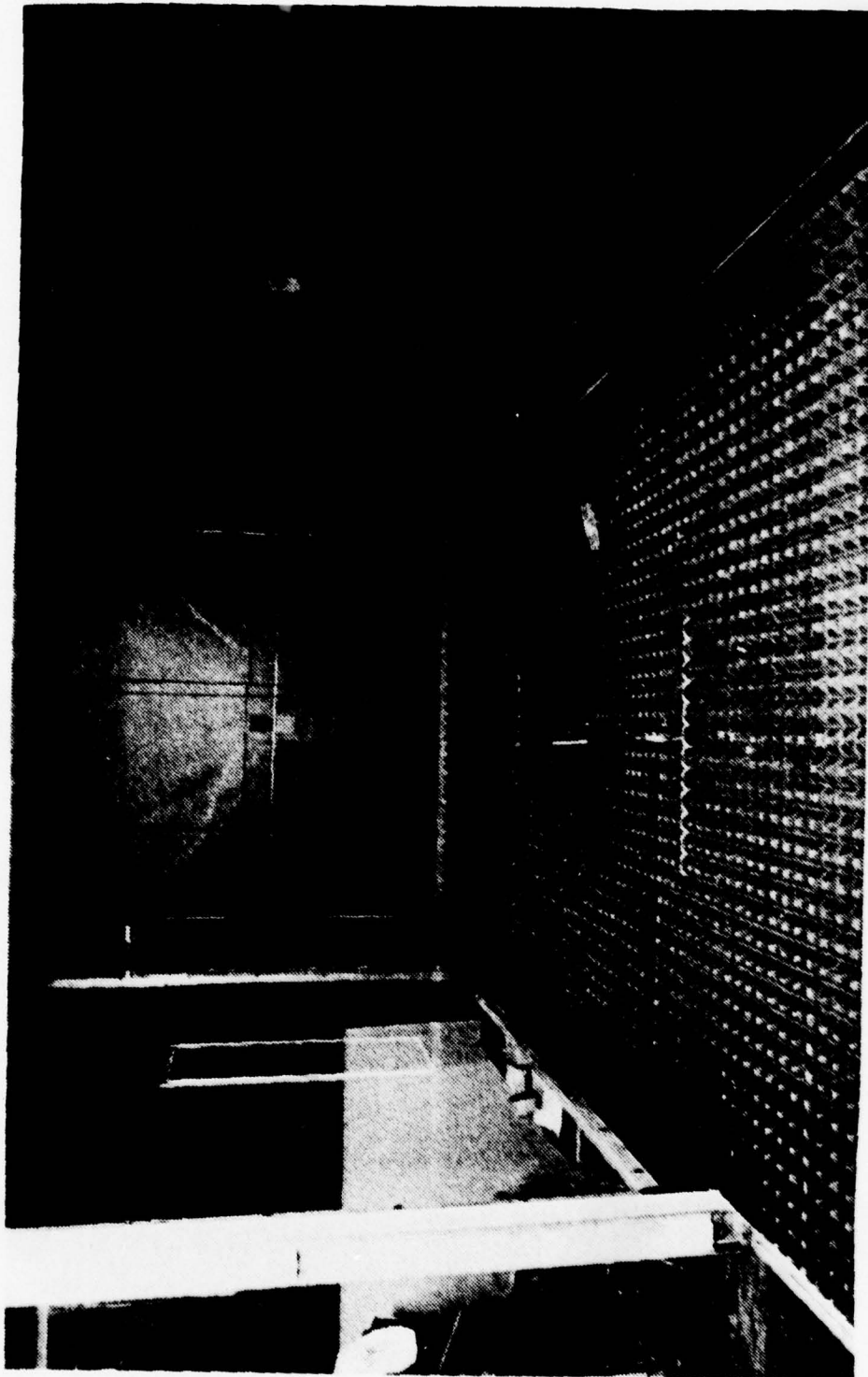
Figure 1

Low Speed Wind Tunnel and Roughness Elements
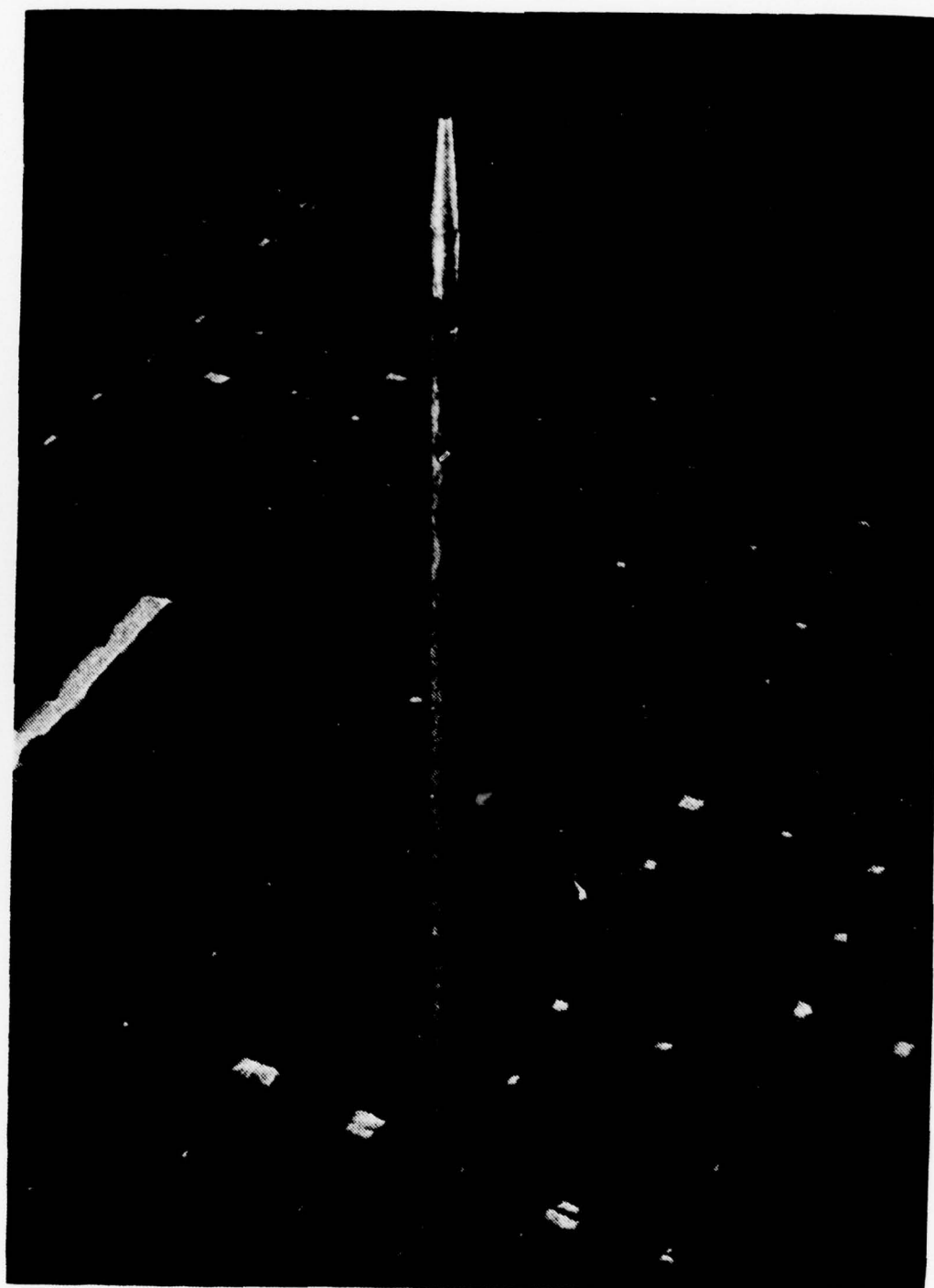
Figure 2

Single Hotwire Probe
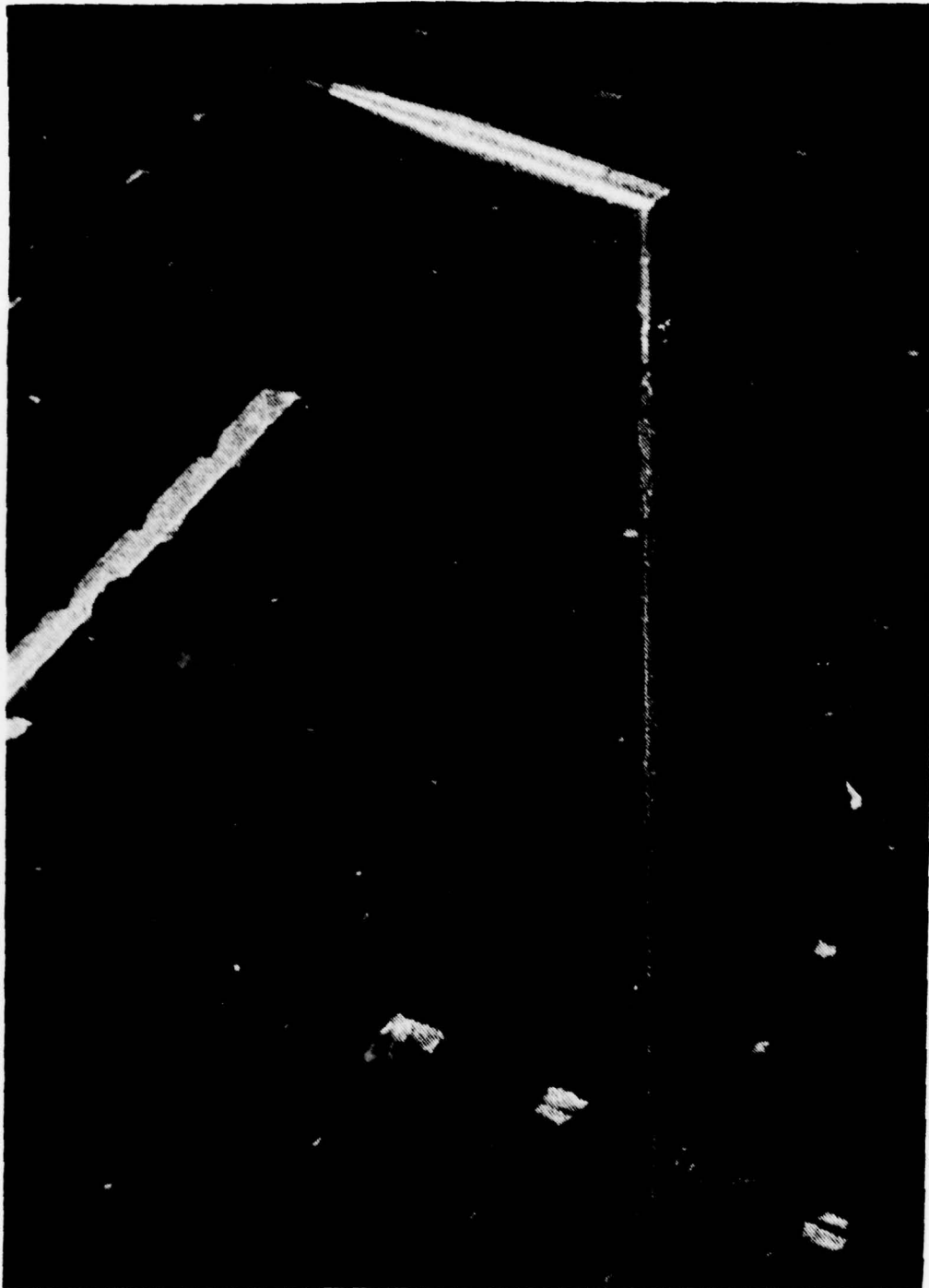
Figure 3
Cross Hotwire Probe

35
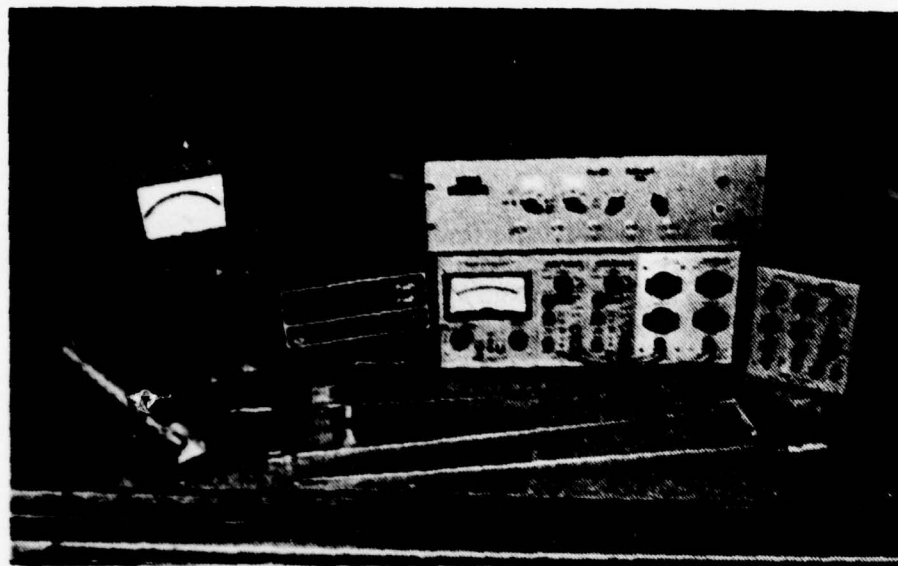
Figure 4

Anemometer and Correlator
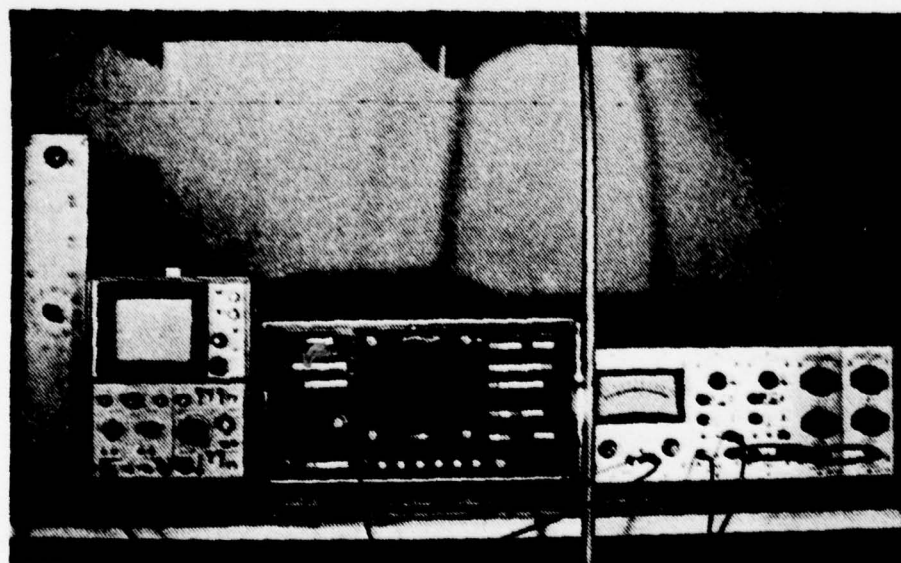
Figure 5

Frequency Counter

Figure 6
Velocimeter

Slope = 0.3402
z_o = 0.0215
$(u_*/U_\infty)^2$ = 0.0035
u_* = 2.319

LOG z
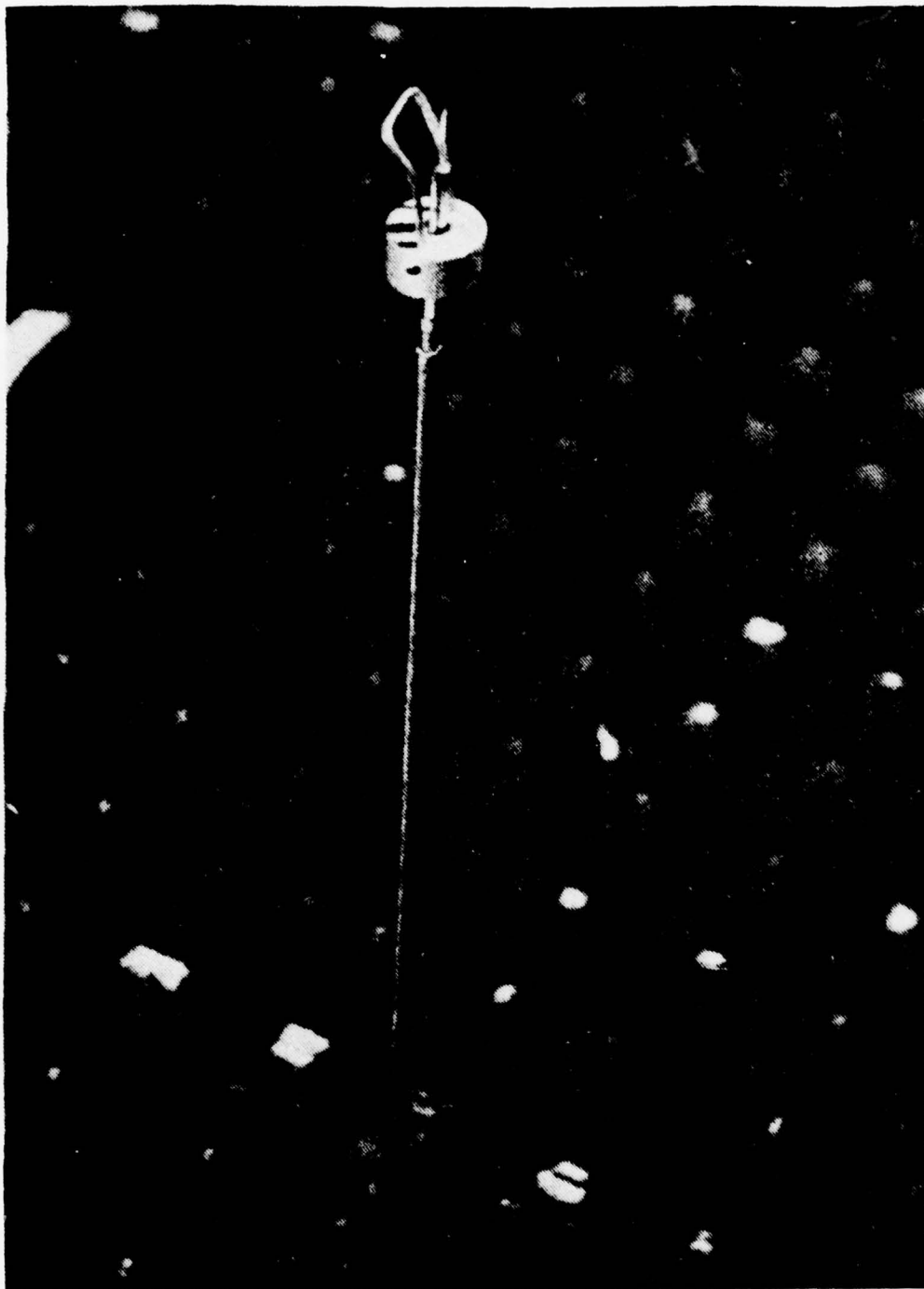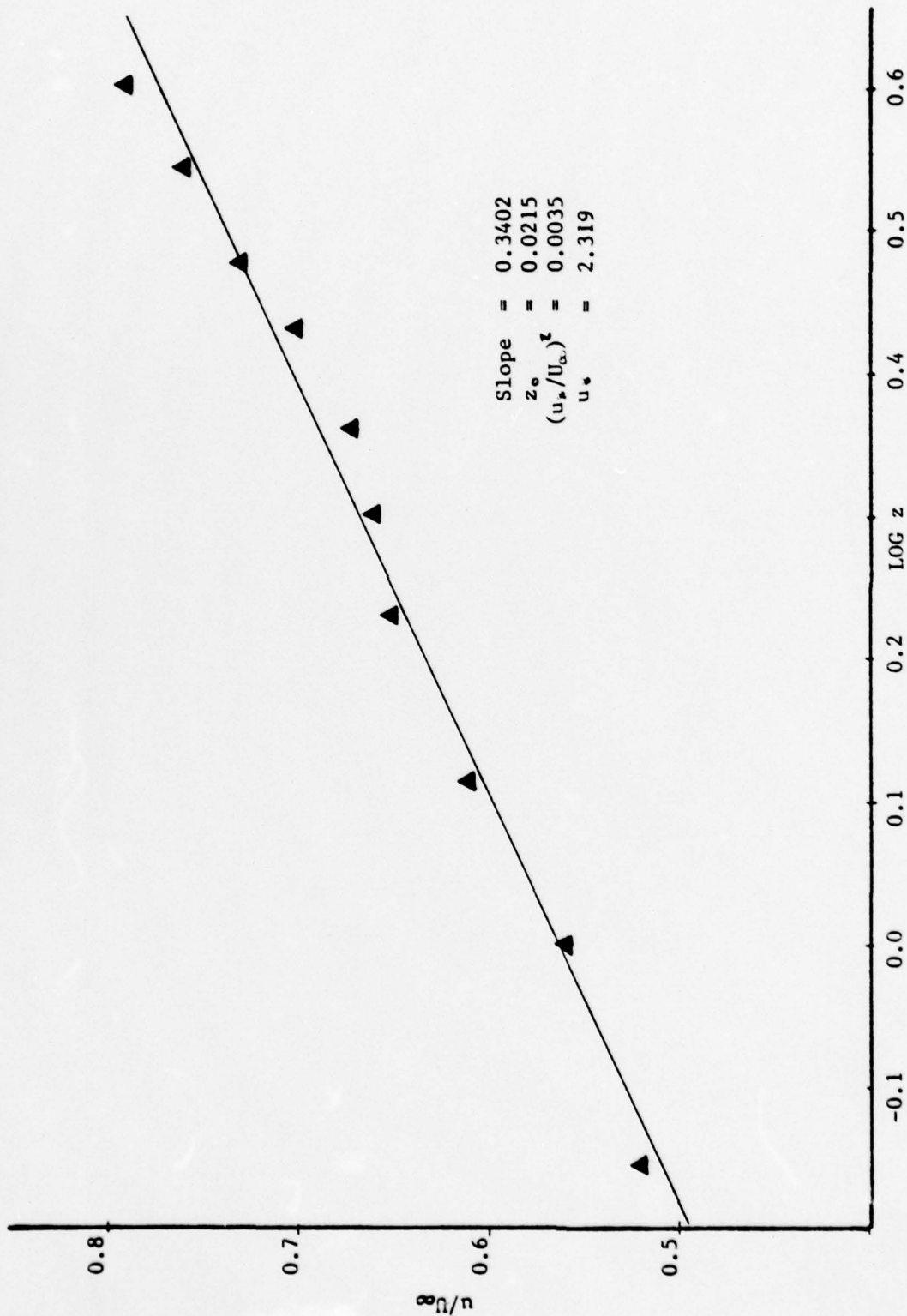
Figure 7

Velocity Profile at 72 Inches Downwind

u/U_∞

38
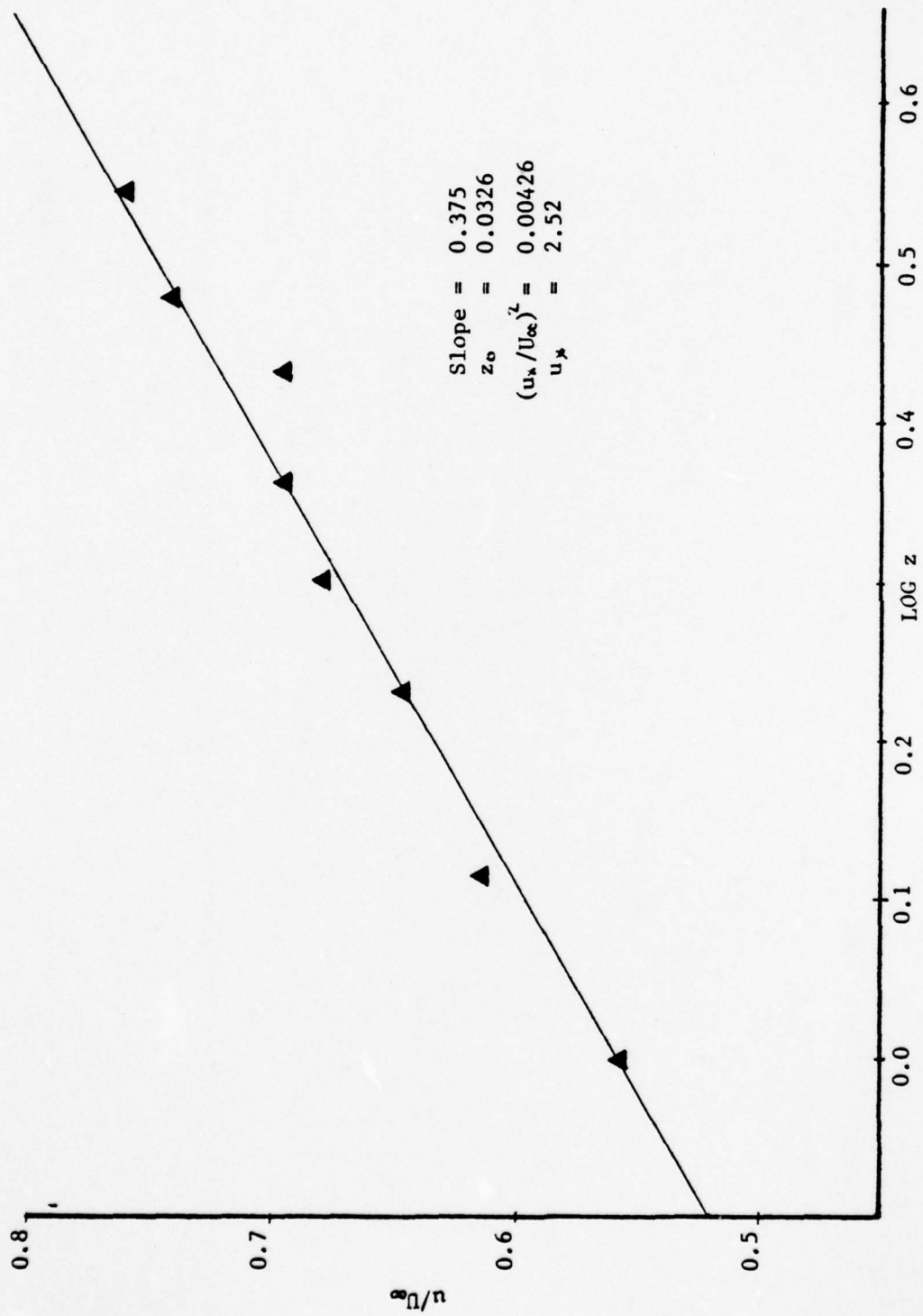
Figure 8

Velocity Profile at 109 inches Downwind

Slope = 0.375
z_0 = 0.0326
$(u_*/U_\infty)^2$ = 0.00426
u_* = 2.52

LOG z

u/U_∞
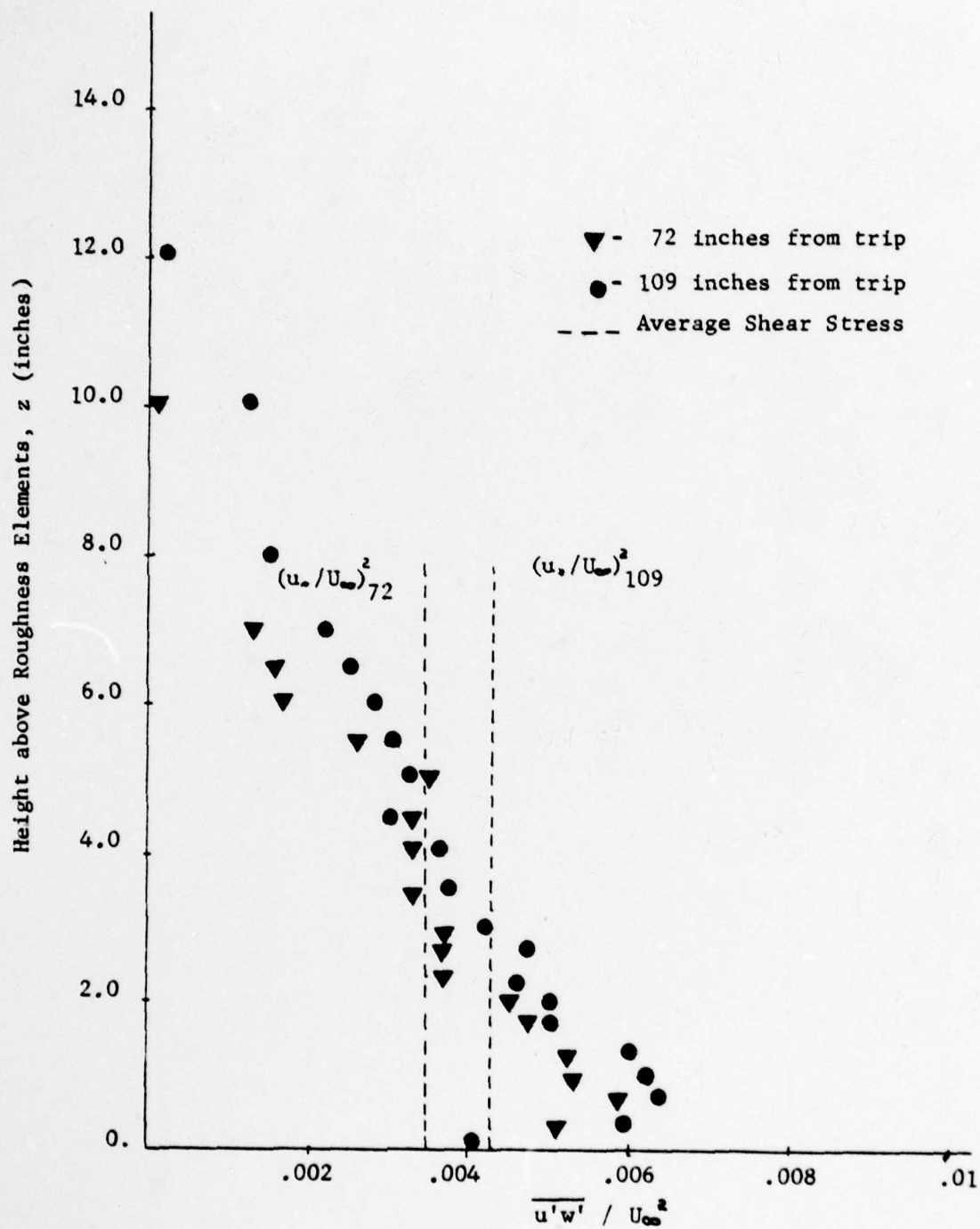
Figure 9
Vertical Distribution of Shear Stress at
72 and 109 inches Downwind
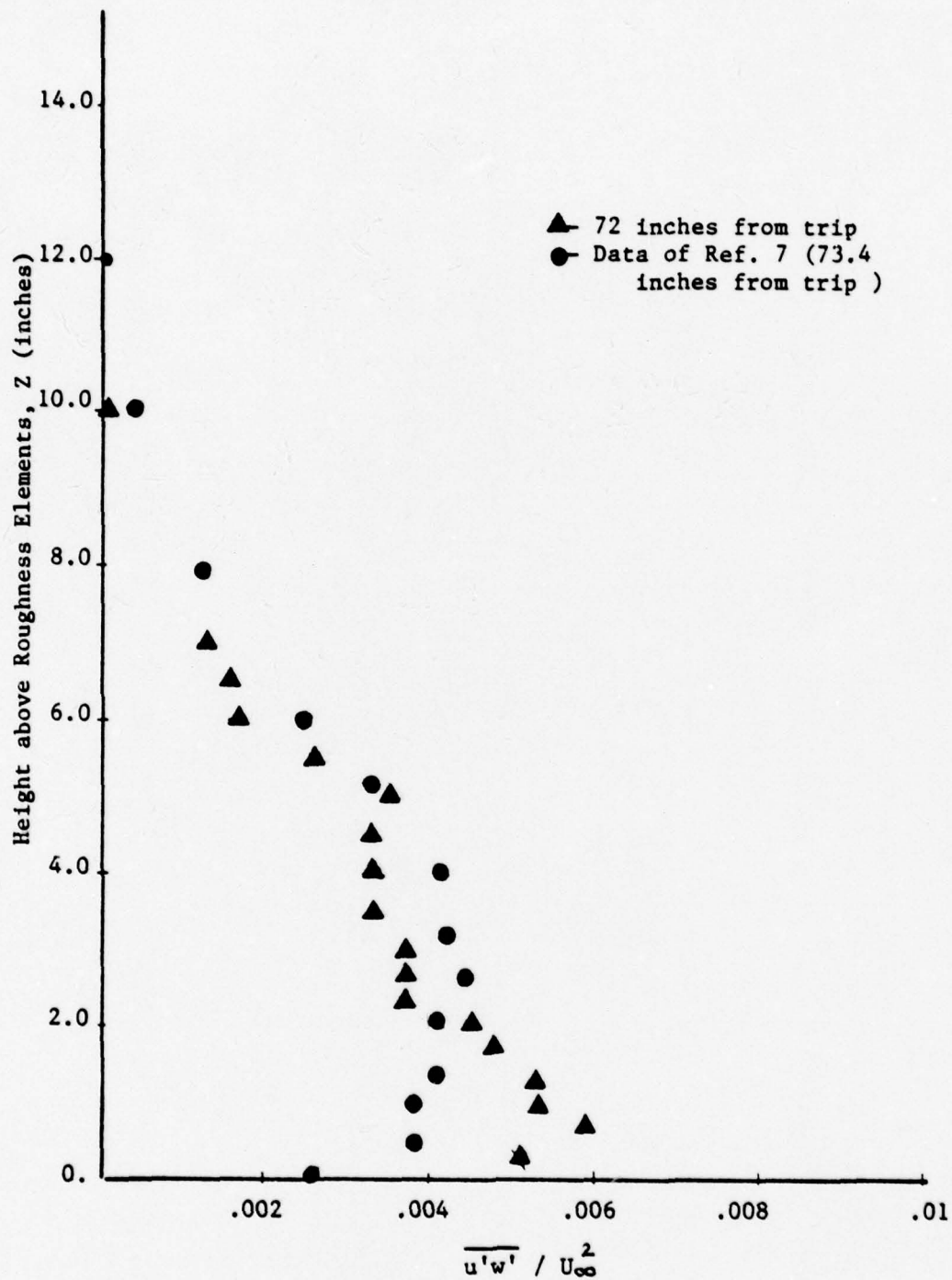
Figure 10
Vertical Distribution of Shear Stress at
72 inches Downwind Compared to the Data of Ref. 7

41
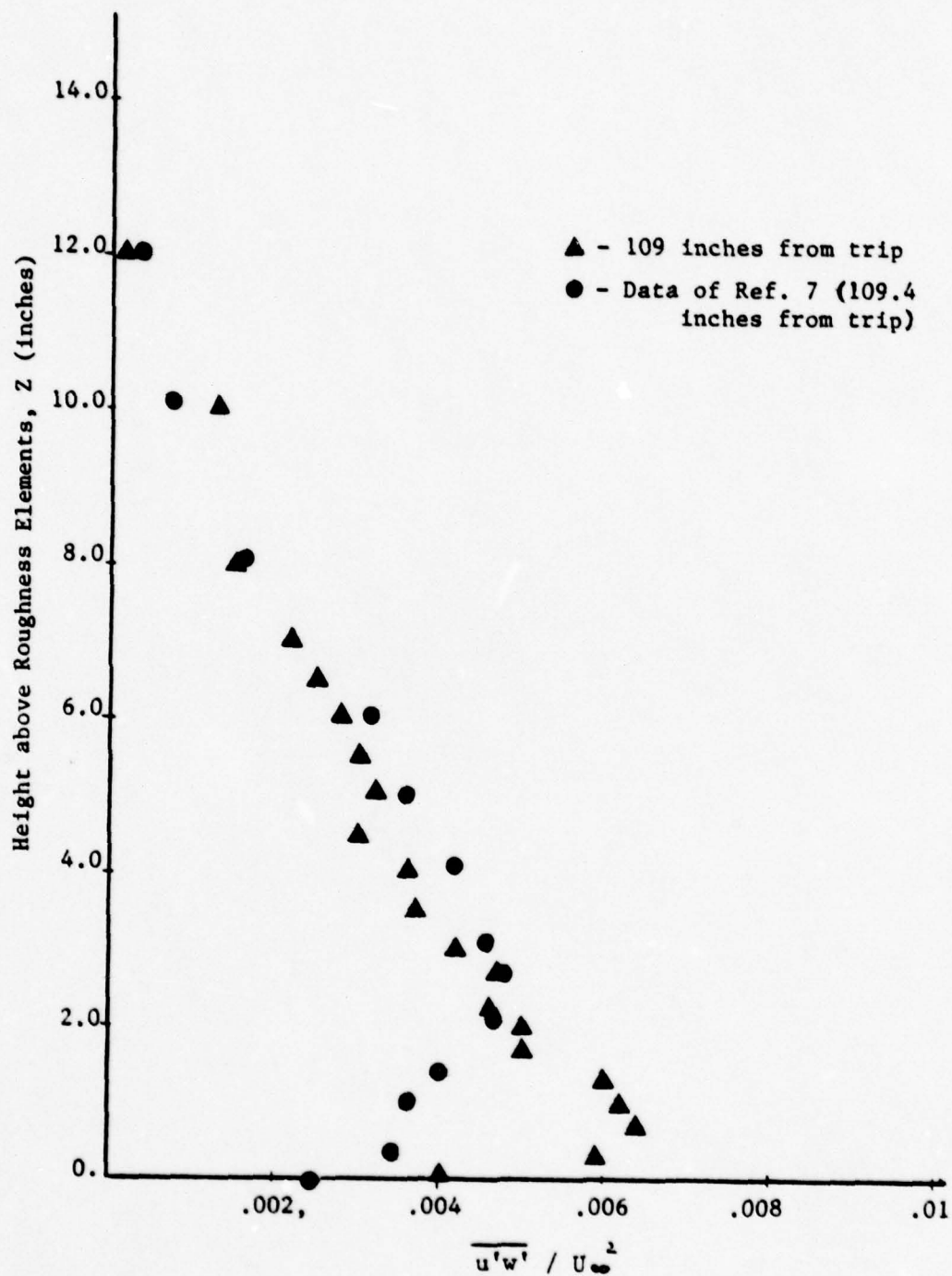
Figure 11
Vertical Distribution of Shear Stress at
109 inches Downwind Compared to the Data of Ref. 7

42
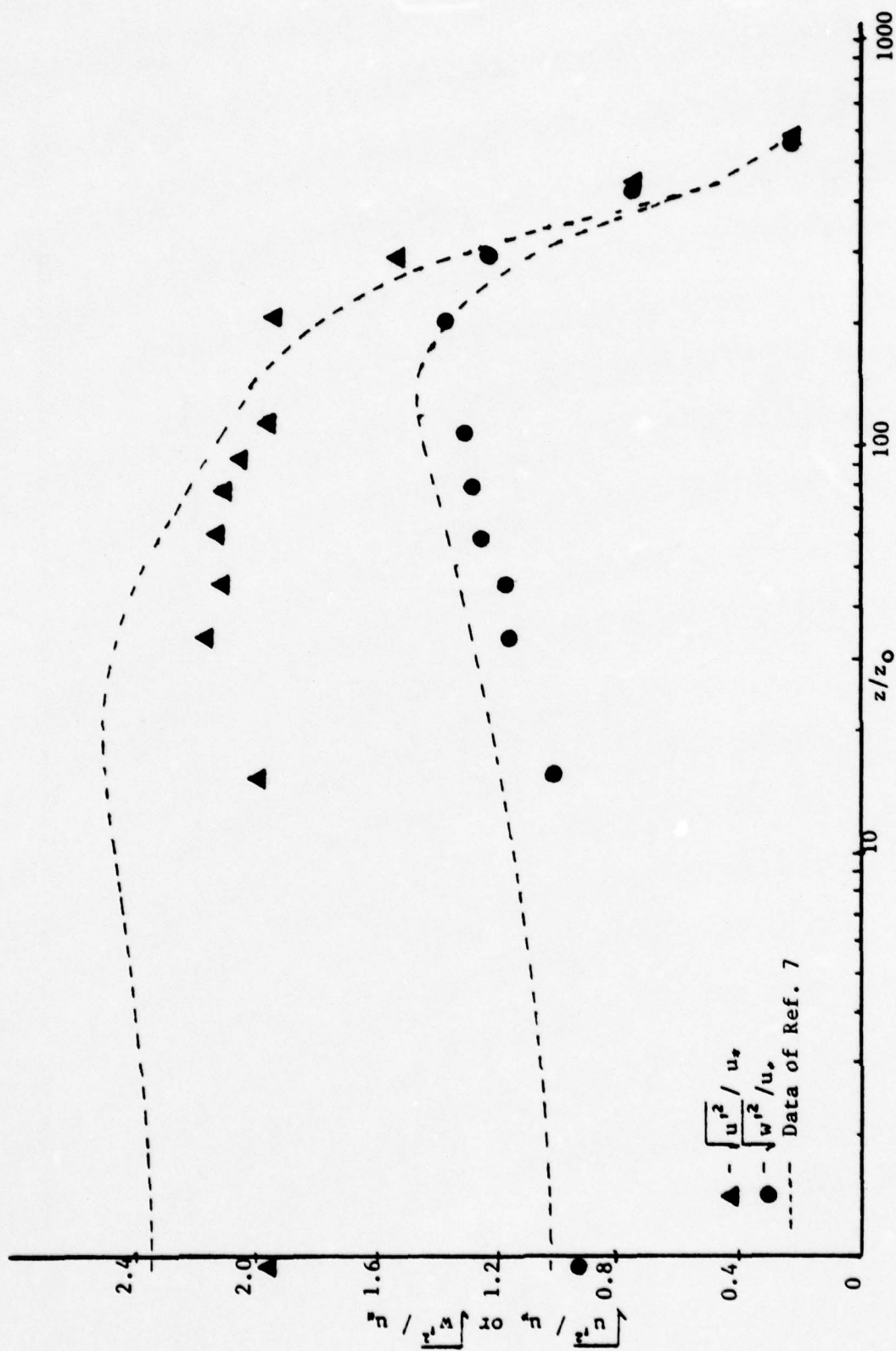
Figure 12
Comparison of Turbulence Intensities at
72 inches Downwind to the Data of Ref. 7
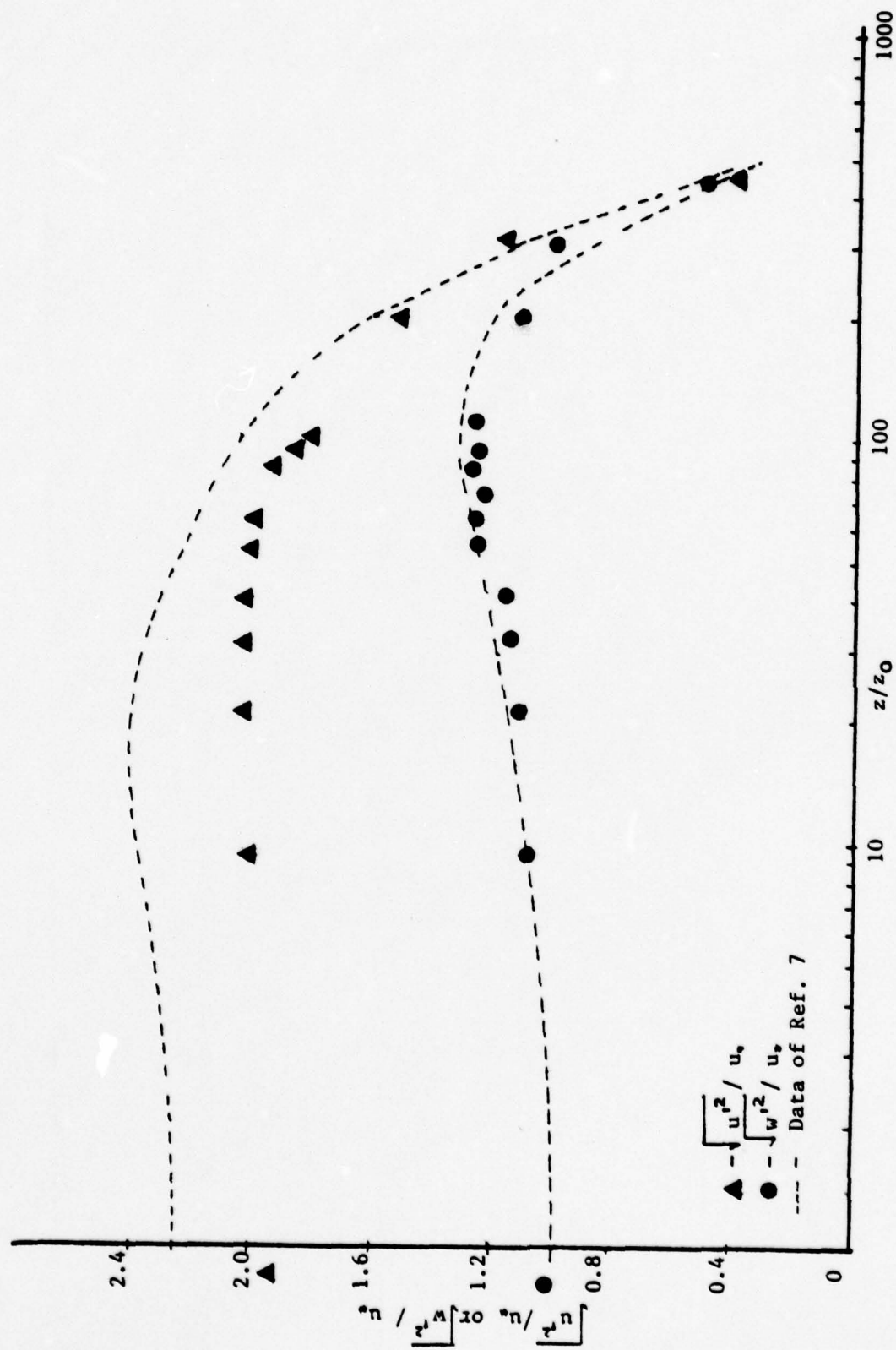
Figure 13
Comparison of Turbulence Intensities at
109 inches to the Data of Ref. 7

44

III.   SIMULATED JET DISPERSION IN A WIND TUNNEL

A.   BACKGROUND

The AQAM model treats most aircraft emissions as finite
line sources. Aircraft engine test cells and run up stands
are treated as point sources. Line sources are modeled by a
general line source or puff type model (Ref. 1-3). Point
sources are modeled by the application of Gaussian plume
theory. This theory represents the downwind concentration of
pollutants from an elevated source as Gaussian distributions
in both the horizontal and vertical directions. When
applied to aircraft exhausts, the line source method first
assumes that the emissions from the moving aircraft come to
rest relative to the ambient wind after a penetration length
due to the velocity effects of the jet. After coming to
rest, the line source is generally ·segmented. The segmented
portions of the line source are then assumed to behave as
pseudo-upwind line sources which are dispersed downwind in a
Gaussian manner. Both methods of modeling use dispersion
coefficients σ_y and σ_z which are the standard deviation
points of a Gaussian or normal distribution curve and are
described by Turner in his workbook on dispersion
estimations (Ref. 16). As mentioned earlier, the dispersion
coefficients are based on the atmospheric stability class

and the time or distance traveled downwind from a relatively
low velocity source.   The applicability of these
coefficients relative to a high velocity, horizontally
emitted source, such as a turbojet engine, was investigated
for various jet parameters.

B.   EQUIPMENT

1. General Discussion

The investigation was conducted in the low speed
wind tunnel described in the previous section. A
burner/nozzle system provided the source for a simulated jet
exhaust. The temperature profile of the exhaust was
measured since it was assumed that mass and temperature are
dispersed by the same mechanism. The temperature profiles
were obtained in the vertical and horizontal directions
using a thermocouple apparatus.

2. Burner/Nozzle

Oxygen and ethylene were mixed and ignited at the
entrance to a burner can, figure 14. The mixture was
augmented with low pressure air for burner cooling and to
create the desired flow rates. The hot gases were
discharged through a 1/8 inch diameter stainless steel tube

into the flow within the wind tunnel. The tube was inserted through the tunnel floor. It was made with one 90 degree bend which aligned the exhaust parallel to the tunnel floor. A nozzle was created by reducing the exit diameter of the tubing to 0.058 inches. The tube was positioned 3 inches above the roughness elements. This position was chosen since it was about the center of the area of constant shear stress discussed in the atmospheric simulation section of this report. Stagnation pressure and temperature probes were used to determine the nozzle exit conditions. The nozzle entered the wind tunnel at a position 72 inches downstream from the boundary layer trip described in the previous section.

3.   Temperature Measuring

Horizontal and vertical temperature profiles were obtained using a chromel-alumel thermocouple probe. The thermocouple was referenced to an Omega electronic Miniature Cold Junction (MCJ). The nozzle and thermocouple system is shown in figure 15. A probe holder and a traverse system permitted positioning of the thermocouple probe in varying axial, transverse, and vertical locations. The traverse system, an electrical-mechanical device mounted under the wind tunnel (fig. 16), facilitated positioning in the vertical and transverse direction. The probe holder,

mounted on the traverse system, permitted the thermocouple probe to be positioned in the axial direction. Two X-Y plotters (fig. 17) were used to record the temperature profiles as a function of downwind distance. One plotter was used for the vertical temperature profile and the other one was used for the horizontal temperature profile. Each plotter was calibrated for displacement in inches and temperature in milli-volts.

C. DISCUSSION OF RESULTS

1. Introduction

The dispersion data from the experimental jet exhaust were used to determine 1) if the plume dispersion was Gaussian, 2) the sensitivity of the jet dispersion to the wind direction, 3) the sensitivity of the jet exhaust dispersion to nozzle exit Mach number (choked and unchoked) under no-wind and wind conditions, 4) the sensitivity of the jet dispersion to upwind nozzle surface blockage and 5) the effect of increased jet exhaust exit temperature on plume rise. The first four items were investigated with an exhaust stagnation temperature at 550 degrees F while the stagnation temperature for the plume rise investigation was increased to 700 degrees F. For choked flow the exhaust stagnation pressure was 32 psia. For unchoked flow it was

48

22 psia.

2. Attainment of Gaussian Dispersion

A Gaussian or normal distribution with a mean value
of zero is defined by the equation

$$y = \{1/ (\sqrt{2\pi}\, \sigma)\} \bullet \exp[-.5(x/\sigma)^2]. \qquad (12)$$

A standard normal distribution (fig. 18) is a normal
distribution in which σ is set equal to one. In this case,
the maximun value of the ordinate of equation 12 is $1/\sqrt{2\pi}$
or 0.3989. The value of the ordinate at one standard
deviation, where $x = \sigma$, of equation 12 is 0.242. To
determine whether the measured temperature profiles were
Gaussian the profiles were standardized in the following
manner. For any radial temperature profile the peak
temperature (Tmax) was assumed to be at the mean of
the distribution. That temperature was scaled such that
Tmax/C was equal to 0.3989. The ordinate values of the
temperature profile were then scaled by the factor C. The
ordinate value of the one point, T_σ, of the profile was
determined by; $T_\sigma = C \bullet 0.242$. At this temperature the
width of the temperature plume is equal to 2σ. The

standard deviation which was determined in this manner was used to non-dimensionalize or standardize the abscissa of the temperature profile. The standard deviations are tabulated in Tables I, II and III for each of the conditions of the experiment. The standardized data points were then plotted against a standard normal distribution curve and compared for closeness of fit. Figures 19 through 24 compare the vertical and horizontal temperature profiles for a choked nozzle flow to the standard normal distribution curve. The jet exhaust was oriented at zero degrees incidence to the free stream wind direction. The wind tunnel centerline velocity was 40 feet per second. The different sets of data represent measurements taken at different axial positions downwind from the jet exhaust. The downwind distance was expressed in terms of jet diameters. The plume was near Gaussian after approximately eight jet diameters downstream from the exit plane of the jet for both the horizontal and vertical profiles. The distance required for the profile to become Gaussian appeared to be the result of the expansion process of the fluid as it exited the nozzle. Similar plots were obtained for the other zero incidence conditions shown in Tables I and II. For each case the plume exhibited near Gaussian properties at about eight jet diameters downstream. The dashed line on Tables I and II indicate the position at which the plume exhibited Gaussian characteristics.

As the nozzle was rotated to the wind direction, the jet-wind interactions caused the horizontal profile to be negatively skewed. The degree of skewness diminished as a function of downwind distance as the effect of the jet exit velocity was overcome by the force of the wind. At the point where the wind was the dominant dispersion factor (ie. past the penetration length) the plume again exhibited Gaussian characteristics. Figure 25 compares the data obtained at an axial distance of 1.72 jet diameters for different angles of incidence to the wind. The angles investigated were 29, 45, 67 and 90 degrees and the data were non-dimensionalized in the same manner as discussed previously. The degree of skewness in figure 25 is evident for each angle of incidence when data are compared to the standard normal distribution curve. Similar data for different downwind stations are plotted on figures 26 through 32. The vertical temperature profiles exhibited no skewness and were very nearly Gaussian at each data position. The σ's which were obtained for the vertical and horizontal dispersions are tabulated in Table III. The downwind distance at which the plume became Gaussian is indicated for each angle by a dotted line.

3. <u>Sensitivity of Exhaust Dispersion to Angle of Incidence to the Wind</u>

51

A spatial representation of the jet exhaust as a
function of downwind and horizontal distances from the
centerline of the nozzle are plotted on figure 33 for jet
exhaust angles of incidence to the wind of 29, 45, 67 and 90
degrees. As expected, as the angle of incidence was
increased, the length normal to the wind direction where the
dispersion distribution was essentially uniform (ie. sigma
approaches infinity) increased (in a nonlinear relationship,
fig. 34). The downwind distance at which the plume became
approximately uniformly distributed was extremely sensitive
to the angle of incidence. The downwind distance decreased
quite rapidly as the angle of incidence was increased in an
almost linear relationship (fig. 34). From Table III it can
also be seen that the corresponding sigmas increased
considerably. Quantitative data was attempted for angles of
incidence greater than 90 degrees. The probe could not be
translated further upstream than the 90 degree jet
orientation. At this position, the exhaust of the jet was
completely dispersed. Qualitatively then, as the angles of
incidence were increased, the exit jet momentum and wind
action acted together to rapidly disperse the exhaust in the
downwind direction. The dispersion coefficients were
increased which resulted in a decreased downwind distance
where the plume became uniformly distributed.

4. Sensitivity of Dispersion Rate to Nozzle Exit Mach Number (choked and unchoked), for Wind and No-wind Conditions

Table I presents the results in terms of the size of the one standard deviation point of the plume in jet diameters as a function of downwind distance from the nozzle exit. It can be seen that the plume dimensions were relatively insensitive to varying exit conditions (choked, unchoked and high temperature). The plume dimensions for both the horizontal and vertical directions varied less than one jet diameter between each condition over a downwind distance of about 120 jet diameteres. The data for the unchoked nozzle with wind dispersed about the same as did the choked flow. For choked flow the Mach number at the exit was 1.0. For the unchoked flow the Mach number was about 0.8. Therefore, both had high velocities relative to a typical stack exhaust.

The dispersions from a choked nozzle with and without wind were also measured. The two sets of data for both the horizontal and vertical directions are plotted in figures 35 and 36. It is seen that the dispersion of the plume became affected by the wind structure at about 30 jet diameteres downwind from the nozzle exit. Between the nozzle exit and about 30 jet diameters downstream, the

53

no-wind and wind data compare fairly well with each other.
Further downwind from that position, however, the two curves
diverge. It was apparent then that the exit conditions of
the nozzle (ie. the penetration length) governed the
dispersion of the plume for about the first 30 jet diameters
downwind, and thereafter the dispersion was primarily a
function of the environmental conditions.

5. Effect of Nozzle Surface Blockage

To investigate the effect of flow disturbances
(caused by the tubing upwind of the nozzle) on the
dispersion of the jet exhaust, two different non-heat
conducting disks were separately fitted on the nozzle
tubing. These blockage devices increased the upstream area
relative to the 1/8 inch tubing by a factor of 15 and 75
respectfully. Table II contains the results and it was
observed that upstream blockage had no significant effect on
the dispersion rates. These upstream blockage effects were
apparently dissipated by the time that the jet had
penetrated approximately 30 jet diameters aft of the nozzle.
These data indicate that aircraft configuration may not
significantly affect the jet dispersion for the slowly
moving taxi operation.

6. Sensitivity to Increased Exit Temperature

54

As stated previously, the effect of exit temperature had little effect on the plume dimensions as a function of downwind distance. An investigation of the plume rise was conducted by measuring the distance between the peak temperature point of the temperature profile and the centerline of the nozzle for two exhaust temperatures. The two sets of data are compared as a fuction of downwind distance in figure 37. Because of the small distances it was difficult to make accurate quantitative conclusions with respect to the plume rise. From the data, however, it appeared that the plume rise was about one jet diameter per 100 degrees F change in exit temperature. Equally as interesting as the plume rise was what appeared to be a small degree of looping caused by the turbulent structure of the atmosphere. This phenomenon is shown in figure 37 as a dotted line. The looping phenomenon is also described in reference 6.

D. COMPARISON OF EXPERIMENTAL RESULTS WITH AQAM

The line source dispersion employed for aircraft exhaust jets in AQAM first assumes that the jet exhaust has a penetration length equal to 140 meters (ie. approximately 140 jet diameters). The penetration length is that length

where the velocity effects of the exhaust cease to be a
factor in dispersing the exhaust. Thus, the exhaust
essentially comes to rest with respect to the ambient air
mass. At this distance then, the exhaust is being dispersed
entirely by the action of the wind. At the penetration
length, estimates of the plume´s lateral and vertical
dimensions are made. The lateral width w, and vertical
height Δz then define the dimensions of a line source of
lenth L. The lateral width is assumed to remain constant
over the length of the line. Once the line source has been
defined, the line is generally segmented and dispersed
downwind using the Gaussian theory of dispersion. That is;
from the dimensions of the line source an initial σ_{yo} and σ_{zo}
are determined from empirical relationships $\sigma_{yo} = w/2.4$ and σ_{zo}
$= \Delta z/2.4$ respectively. With these values of σ_{yo} and σ_{zo} an
upwind distance for a pseudo upwind line source is
determined using the σ_y and σ_z vs. distance or time charts
of reference 7. The pollution concentrations are then
dispersed from the determined line source in a Gaussian
manner. If w and Δz are not specified inputs, the AQAM
model uses default values of 20 meters and 8 meters
respectfully.

The penetration length determined in this investigation
for zero degrees orientation to the wind was approximately
30 jet diameters, considerably shorter than the 140 jet

56

diameters of AQAM. The 30 jet diameter figure was further
investigated using the dispersion data from tests with the
nozzle oriented at other than zero degrees to the wind (fig.
38). The 30 jet diameter penetration distance determined
from the axial conditions, indicated by an arc in figure 38,
was compared to the point where the dispersion curves
exhibited no skewness (ie. where the distributions were
Gaussian normal to the wind direction). It was assumed that
beyond this position the jet effects could be neglected and
that the jet would be dispersed by the ambient wind only.
This assumption is not entirely correct since the plume
continued to exhibit horizontal displacements normal to the
wind. Along the jet axis the penetration length increased
as a function of incidence to the wind from about 28 to 58
jet diameters, still considerably less than the 140 jet
diameters assumed by AQAM. This relationship is plotted in
figure 39 and appears to be approximately linear between 29
and 90 degrees relative to the axial orientation. The
distance downwind from the nozzle where the plume became
Gaussian, however, remained approximately constant at 25-30 jet
diameteres. It was also noted that the corresponding σ's at
the Gaussian point for each angle became wider with
increased angles of incidence due to more turbulent mixing.
This relationship is plotted in figure 40. With the limited
number of data points available it appears that the
relationship follows a smooth curve. σ_y and σ_z and the jet

penetration length seem to be predictable between zero and
90 degrees of incidence to the wind for neutral stability
and these nozzle exit conditions. These values could be
used in AQAM to determine w and $\triangle z$ instead of estimating
them or using the default values. The relationship shown in
figure 39 could also be used as input for jet penetration
length. However, since the penetration lengths are small,
it may be better to neglect this effect entirely.

A comparison of the rates of dispersion for zero degrees
incidence to the wind (i.e. the slope of the σ_y and σ_z vs.
distance curves) was made between a neutrally stable
atmosphere (class D) in reference 1 and the experimental
data. As can be seen from figures 35 and 36 the
experimental dispersion rates were greater than the class D
rate used by reference 1 for a neutrally stable atmosphere.
Reference 1 indicated that this may be expected. The
dispersion rates were obtained from data compiled from
typical low velocity stack emissions and not from high
velocity sources. In general terms, it appears that for the
conditions of this experiment, a more realistic
representation of the actual dispersion rate could be
obtained if the atmospheric stability class was decreased by
one.

For a vertical stack, AQAM also predicts the plume rise

due to thermal effects by one of two relationships. These
relationships were investigated to see if they could be used
to predict the plume rise observed in the experiment. For
the HOLLAND plume rise formula, a rise of 0.05 jet diameters
per 100 degrees F was predicted and for the CARSON-MOSES
formula a rise of 0.008 jet diameters was predicted per 100
degrees F. This compares to about 1 jet diameter plume rise
observed in the experiment. Again, the discrepancy seems to
be in the use of equations developed for low velocity
sources for sources with high velocity.
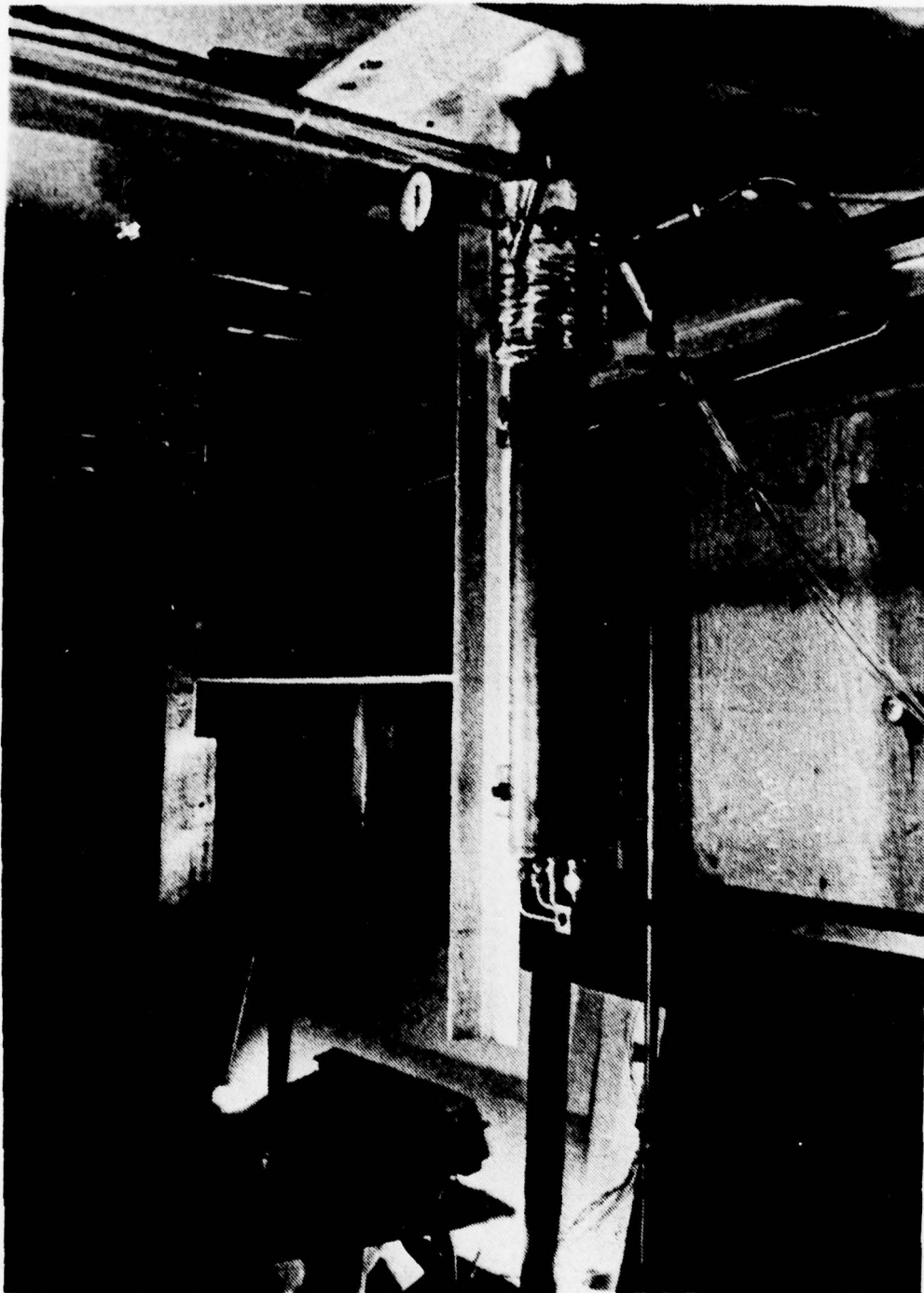
Figure 14
Burner Can

60
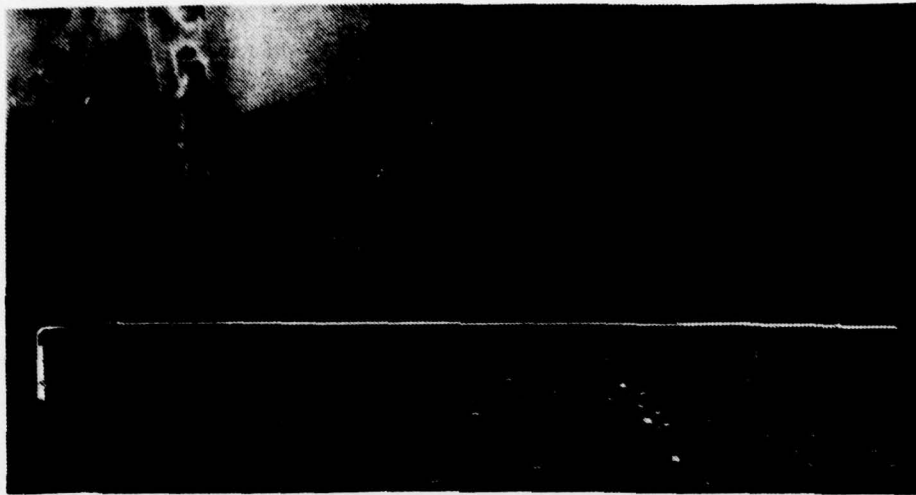
Figure 15
Exhaust Nozzle and Thermocouple Probe
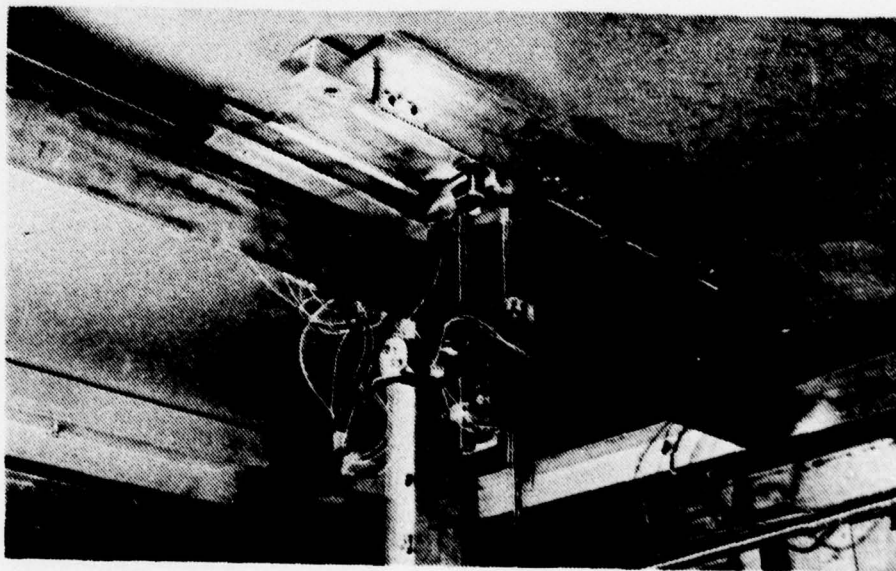
Figure 16
Thermocouple Traverse System
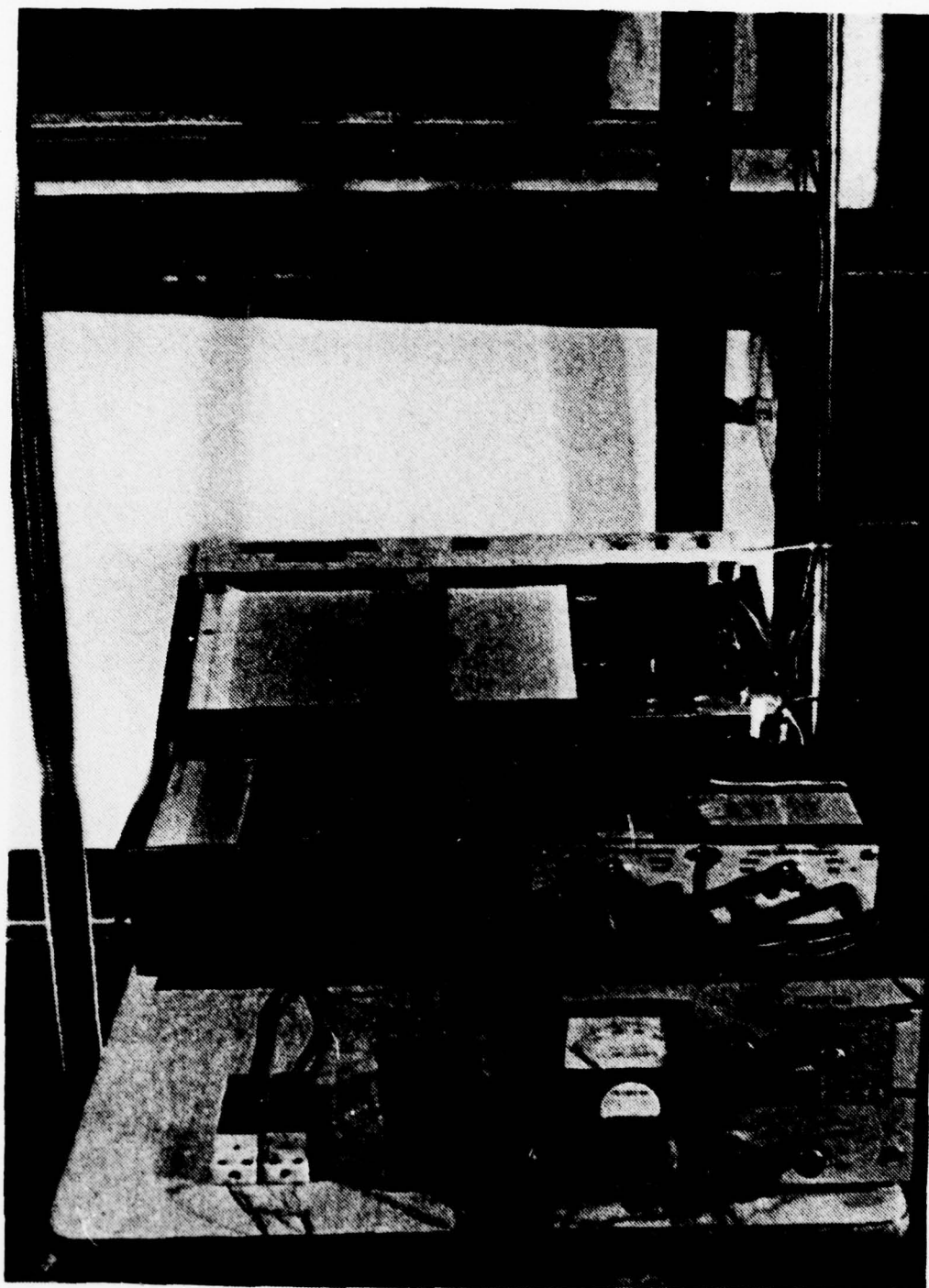
Figure 17
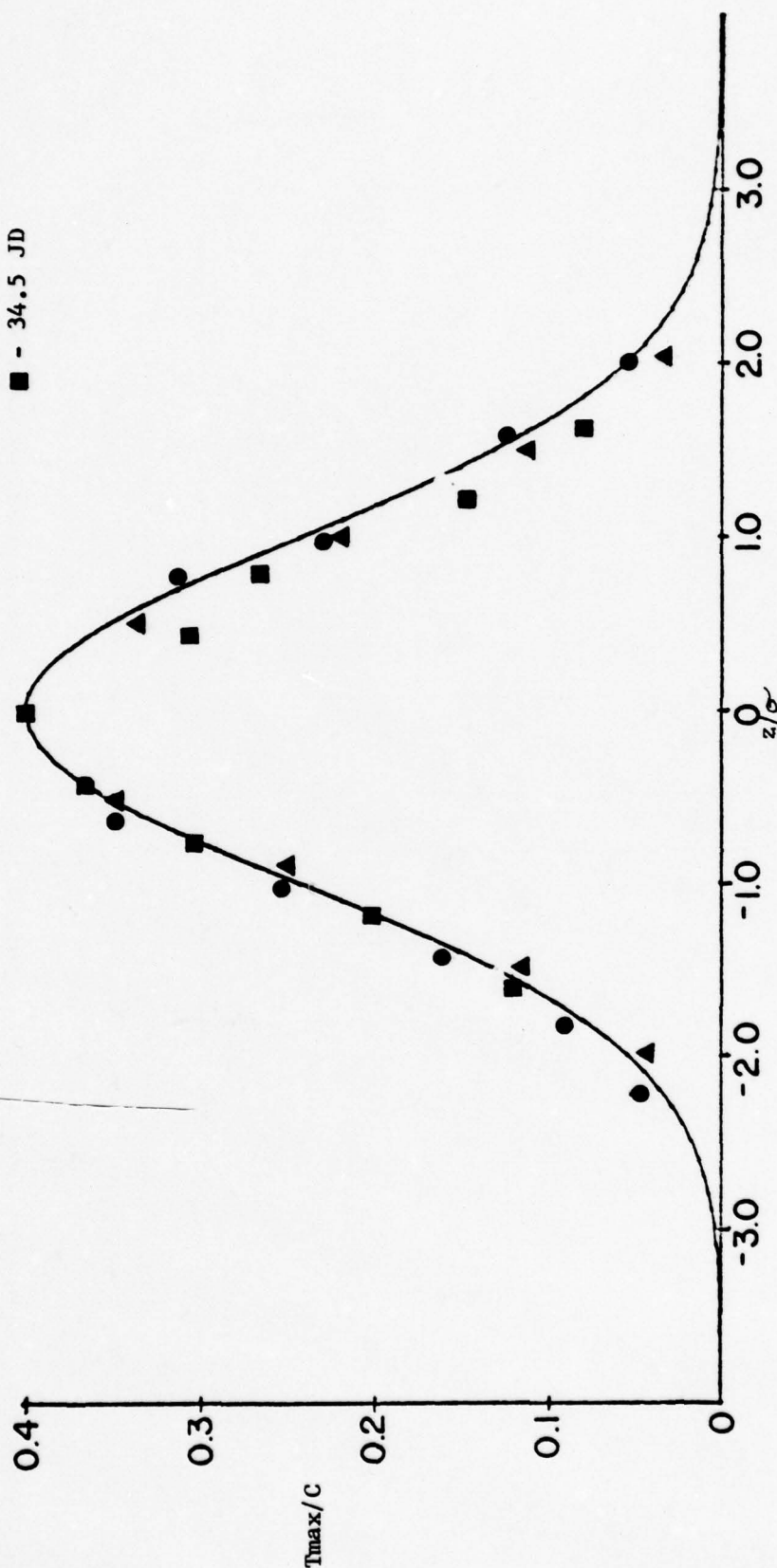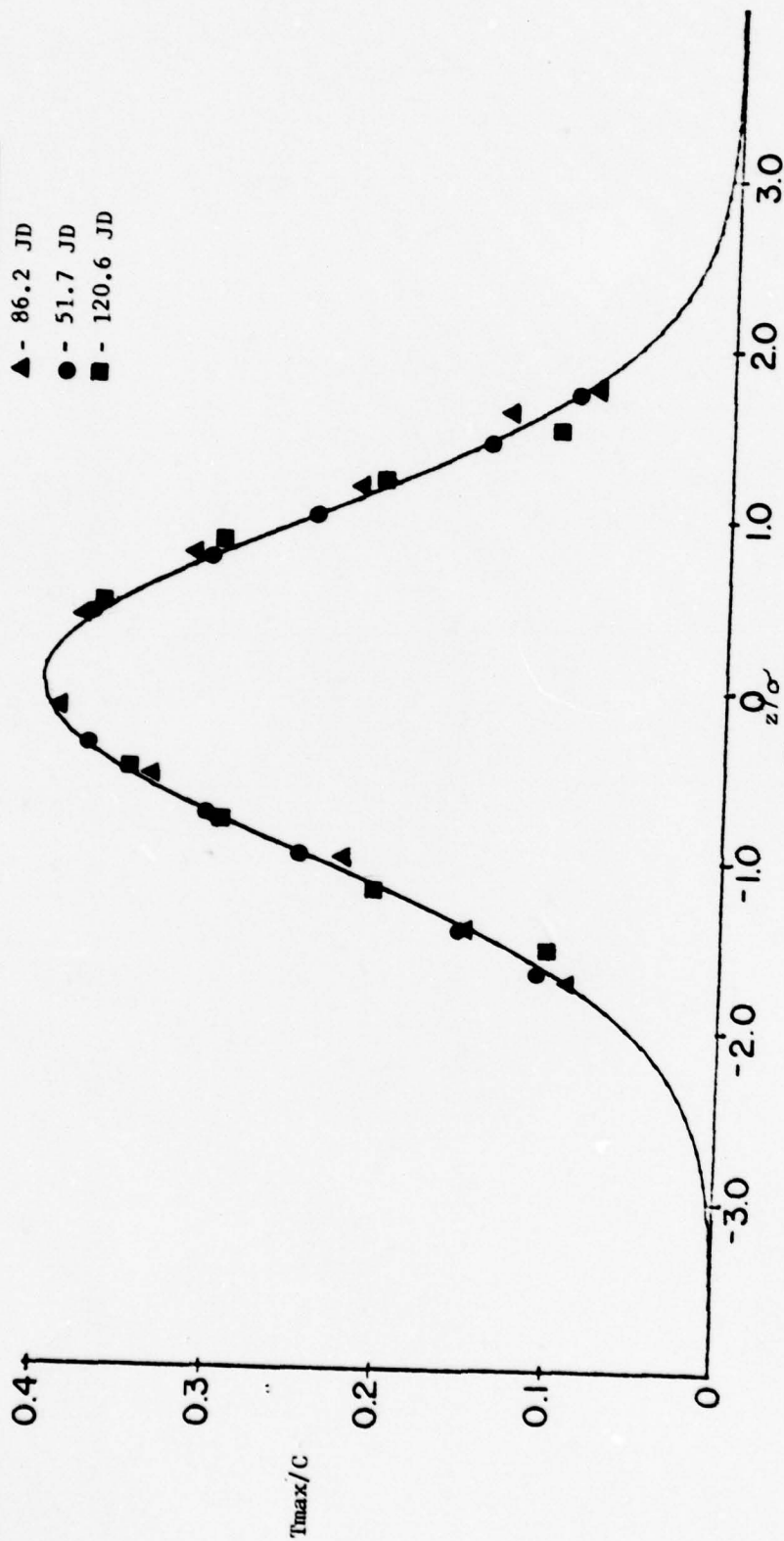X-Y Plotters for Temperature Measuring
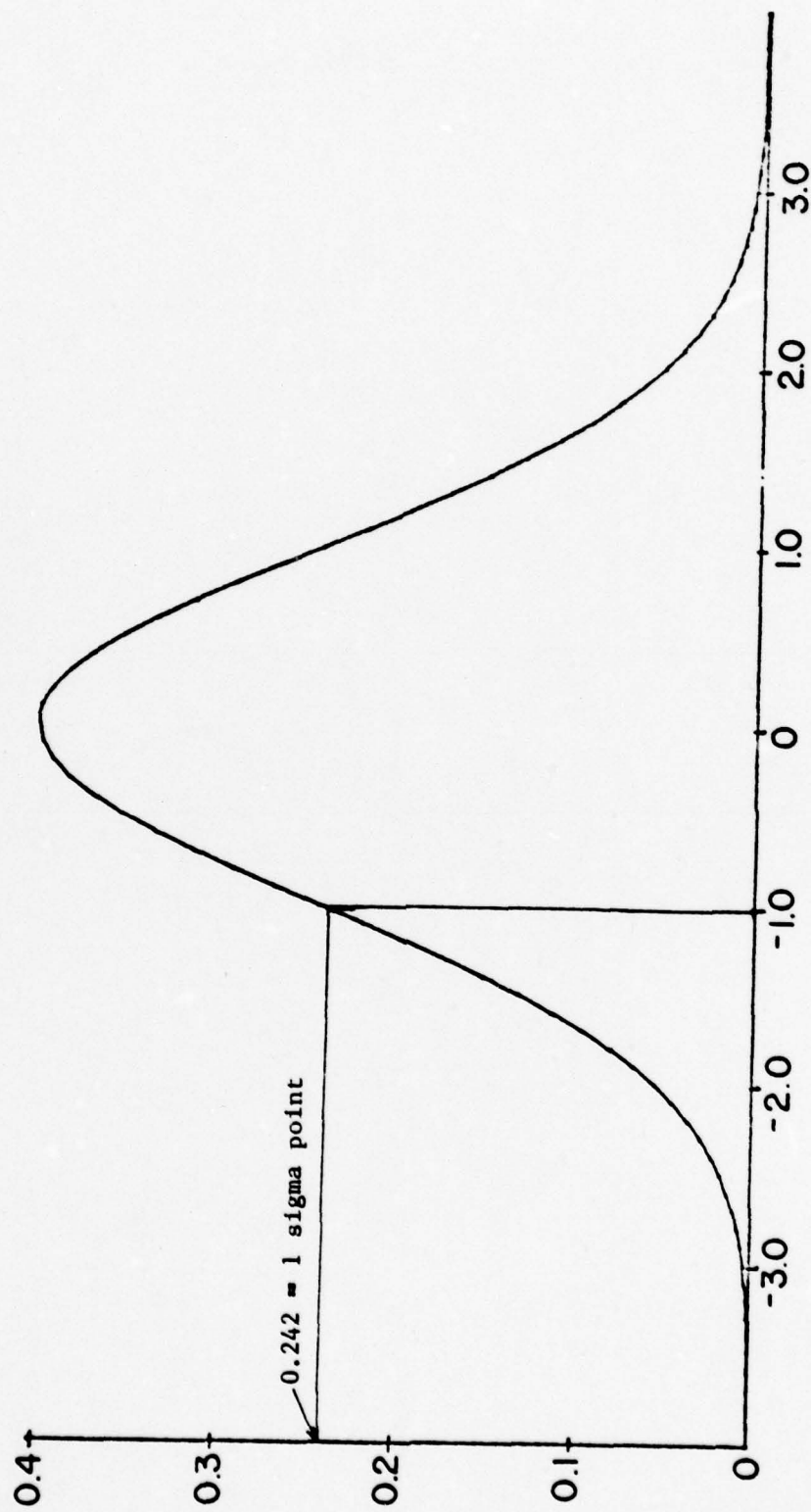
Figure 18

Standard Normal Distribution

63
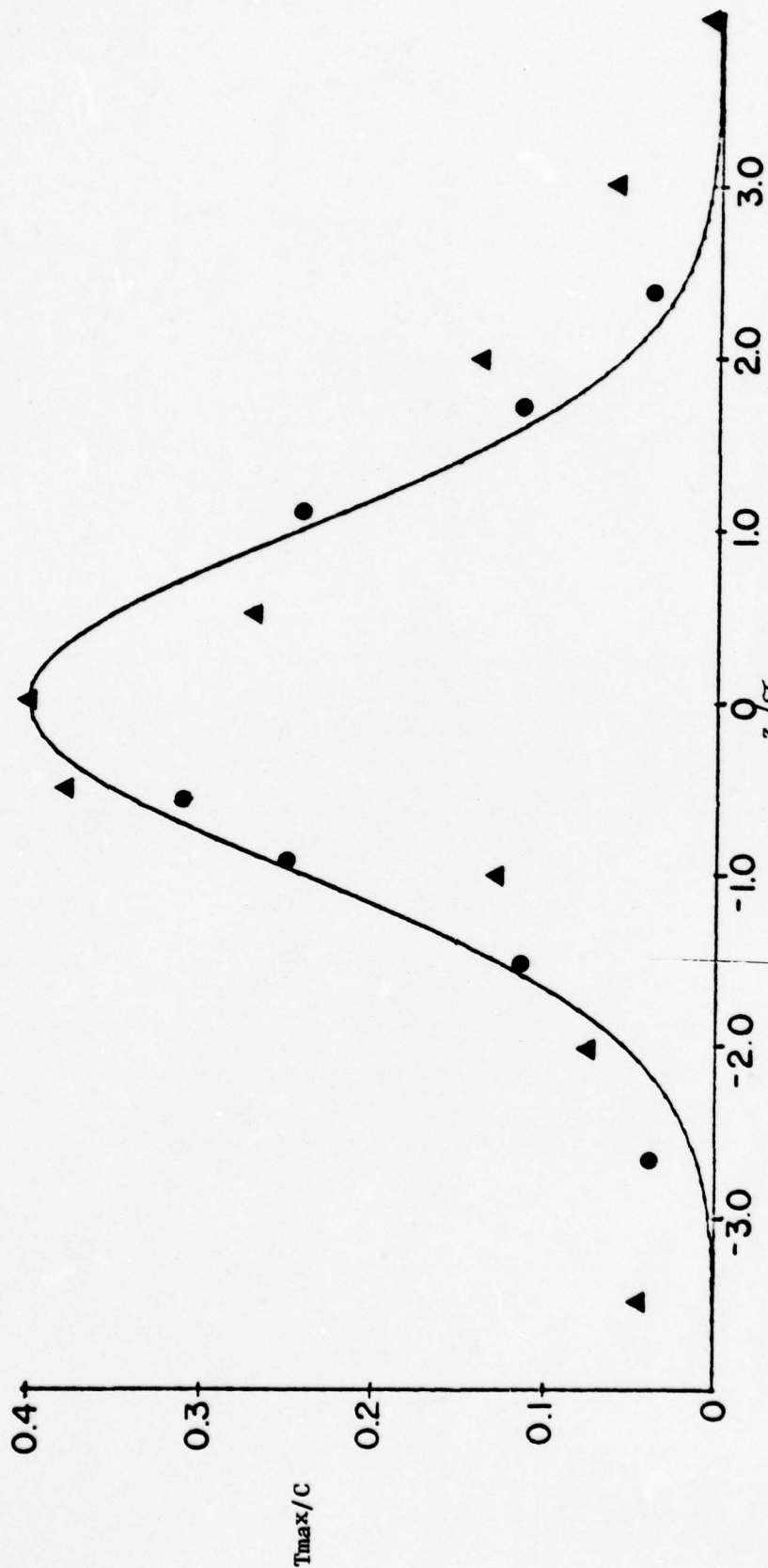
Figure 19
Comparison of Vertical Distribution of
Temperature to a Standard Normal Distribution
for Zero Degrees Angle of Incidence

Figure 20

Comparison of Vertical Distribution of
Temperature to a Standard Normal Distribution
for Zero Degrees Angle of Incidence

Figure 21

Comparison of Vertical Distribution of
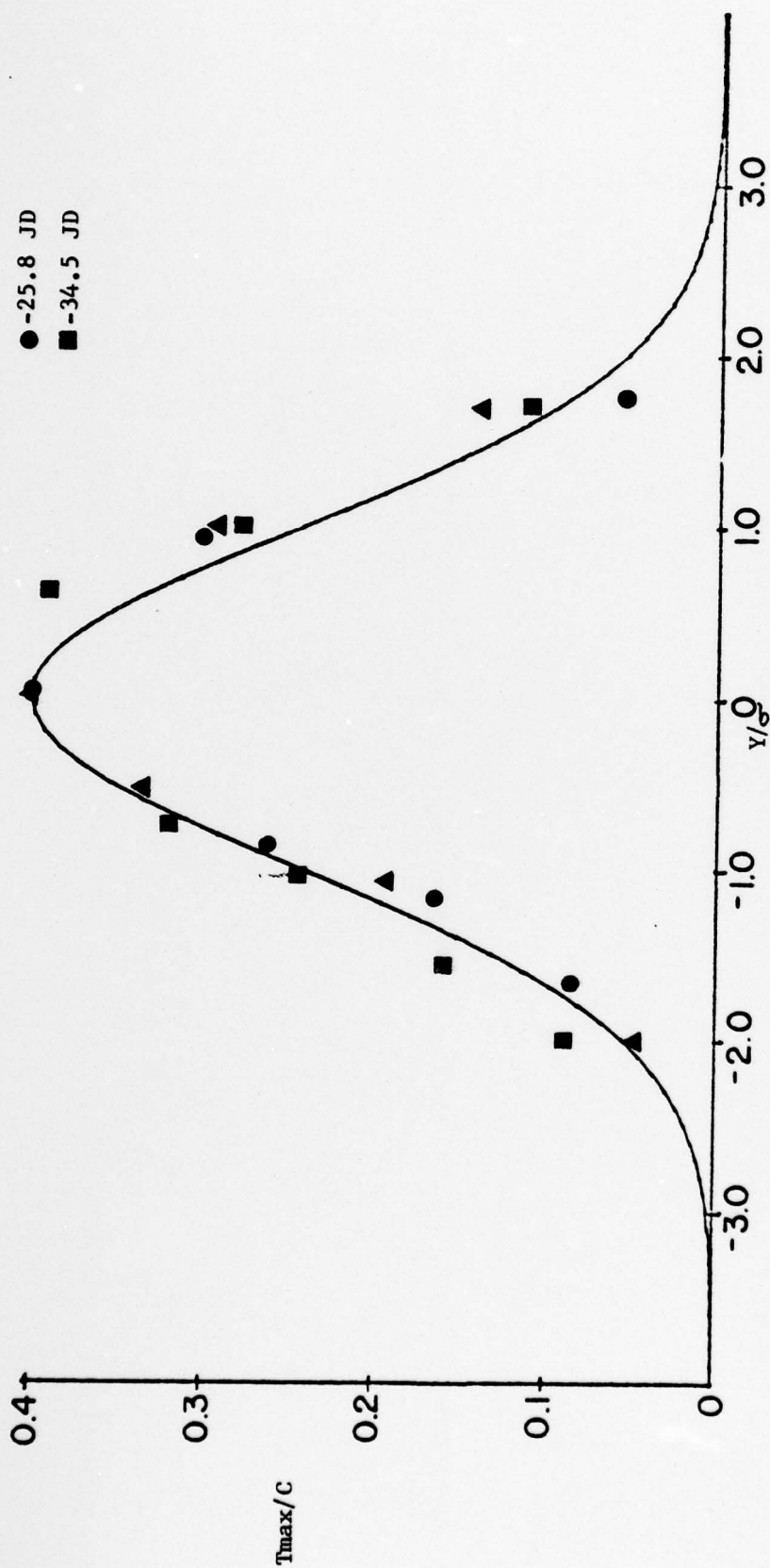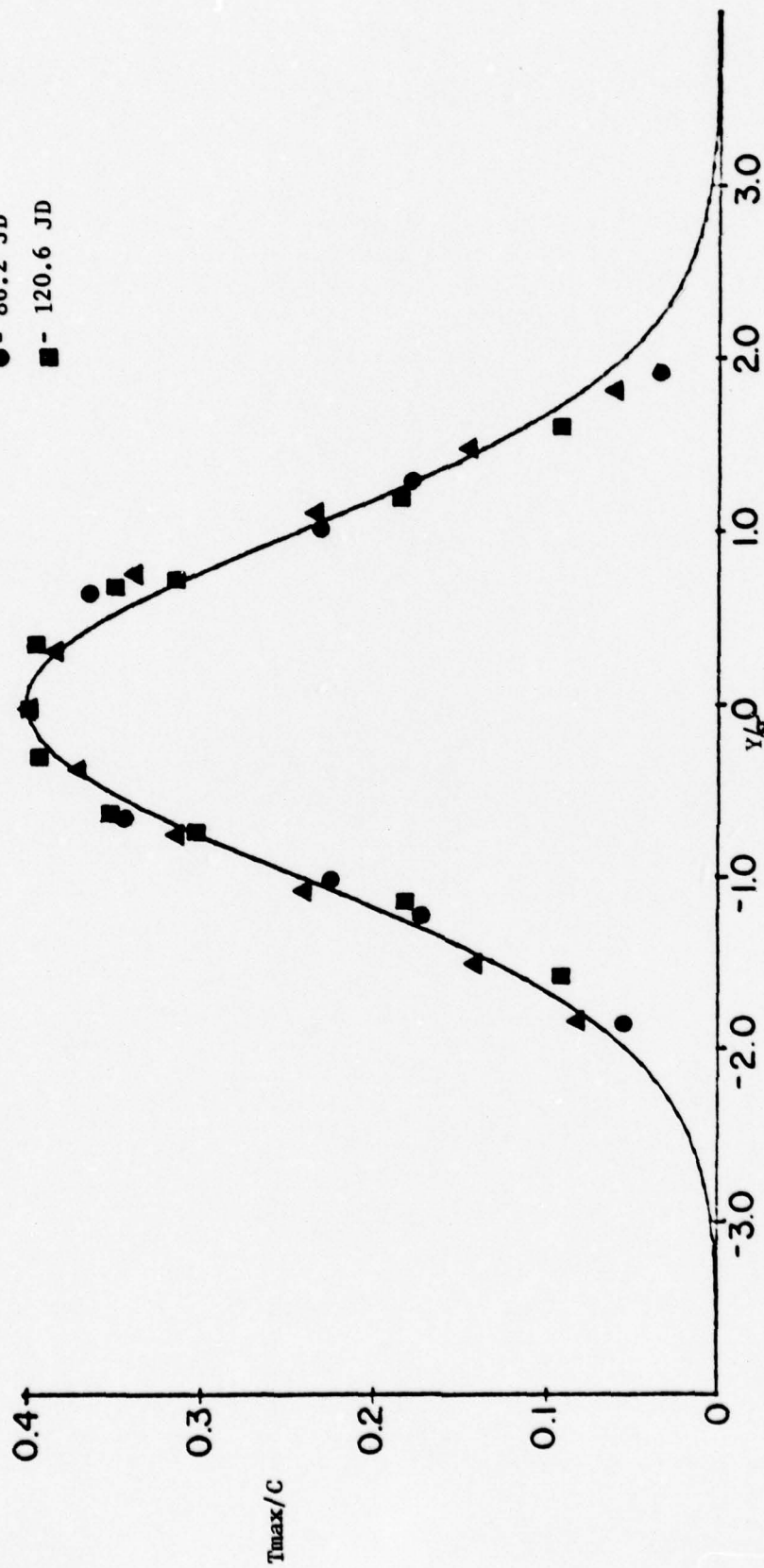Temperature to a Standard Normal Distribution
for Zero Degrees Angle of Incidence
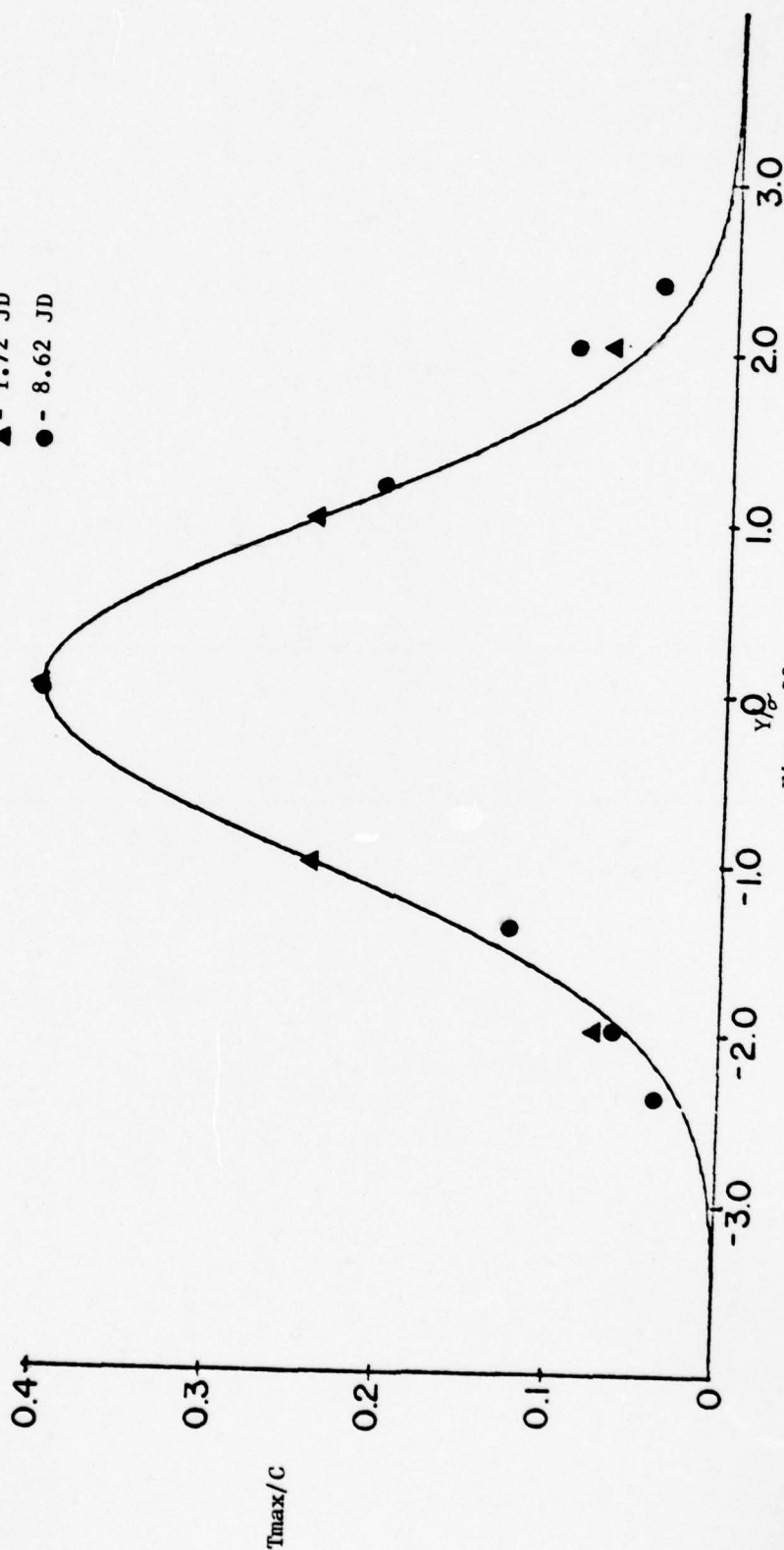
Figure 22
Comparison of Horizontal Distribution of
Temperature to a Standard Normal Distribution
for Zero Angle of Incidence

67

Figure 23

Comparison of Horizontal Distribution of
Temperature to a Standard Normal Distribution
for Zero Angle of Incidence

Figure 24
Comparison of Horizontal Distribution of
Temperature to a Standard Normal Distribution
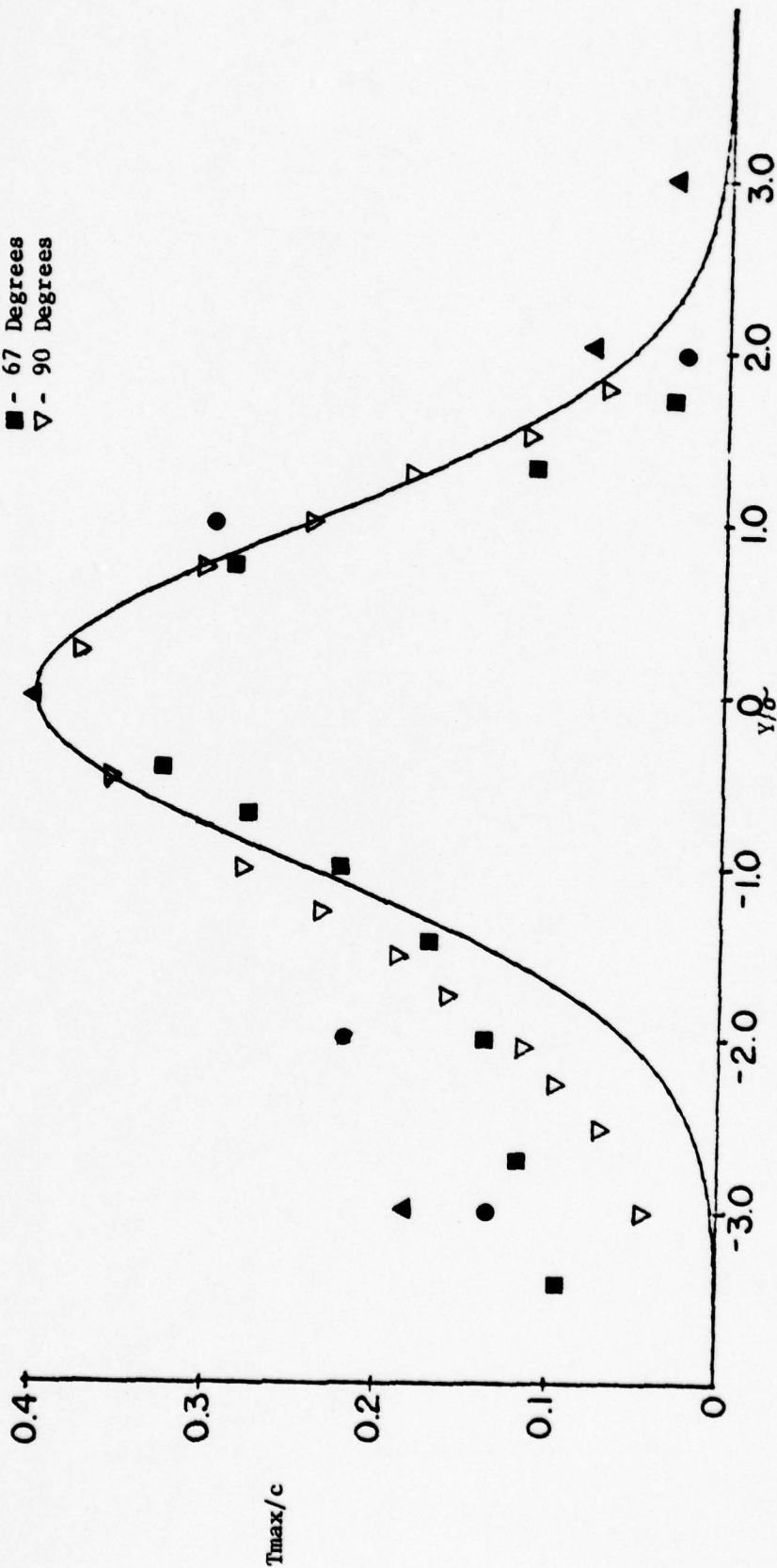for Zero Angle of Incidence

69

Figure 25
Comparison of Horizontal Distribution of Temperature to a
Standard Normal Distribution for Angles of Incidence at
1.72 Jet Diameters Downwind from the Nozzle

Angles of Incidence

▲ - 29 Degrees
● - 45 Degrees
■ - 67 Degrees
▽ - 90 Degrees

T_{max}/c

0.4
0.3
0.2
0.1
0

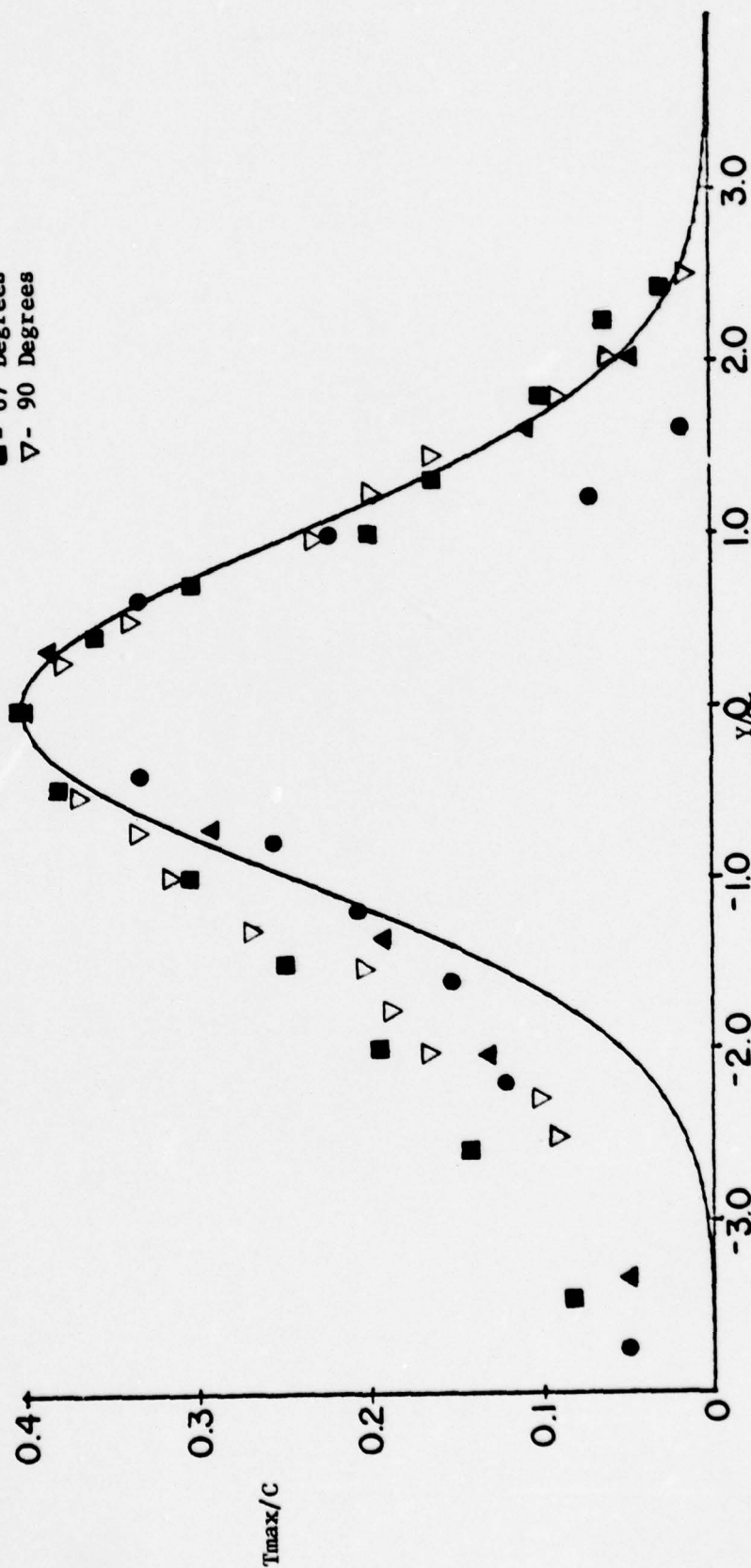-3.0   -2.0   -1.0   0   1.0   2.0   3.0

y/σ

70

Figure 26

Comparison of Horizontal Distribution of Temperature to a
Standard Normal Distribution for Angles of Incidence at
8.62 Jet Diameters Downwind from the Nozzle

71

Figure 27

Comparison of Horizontal Distribution of Temperature to a
Standard Normal Distribution for Angles of Incidence at
17.2 Jet Diameters Downwind from the Nozzle

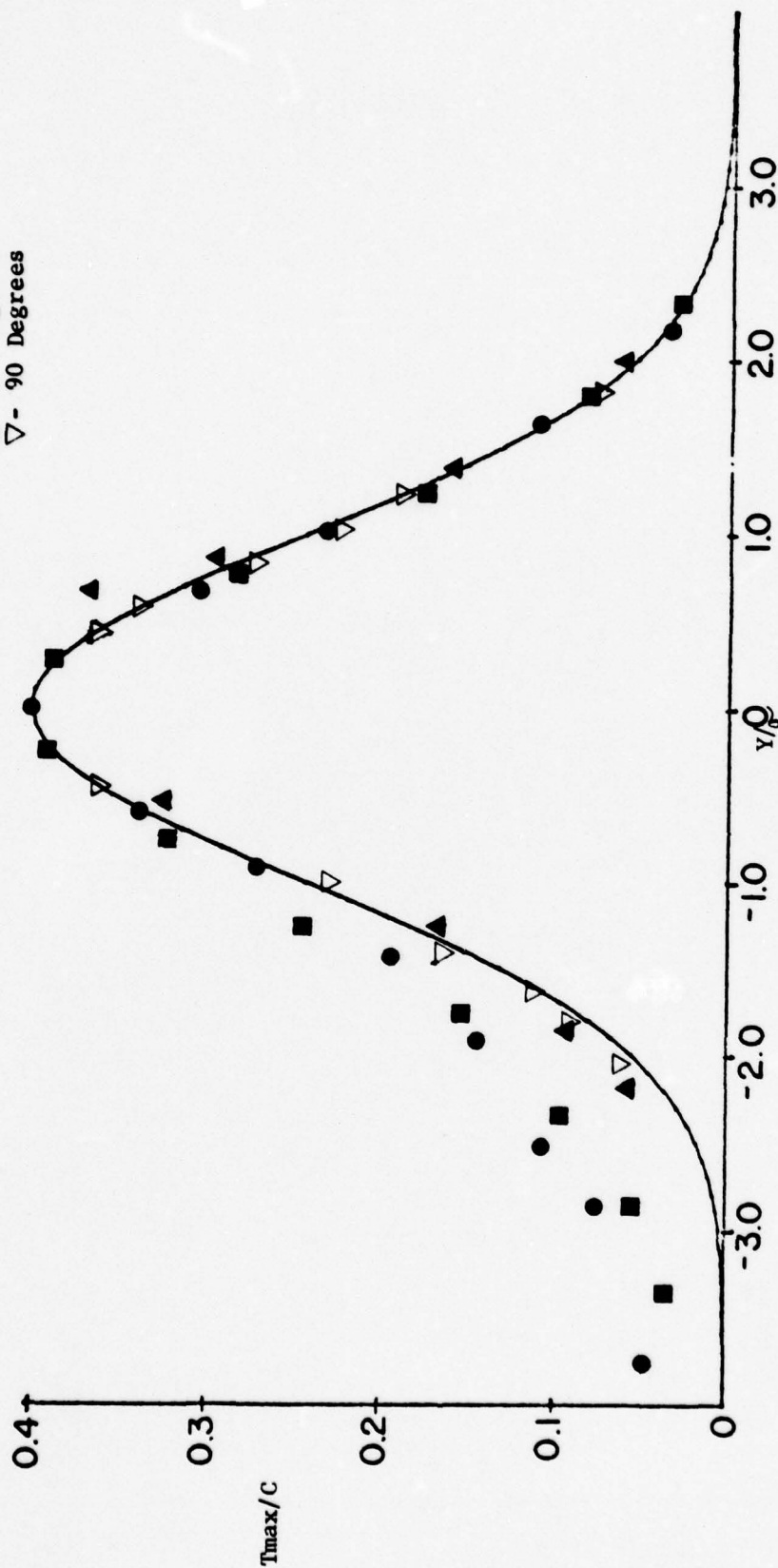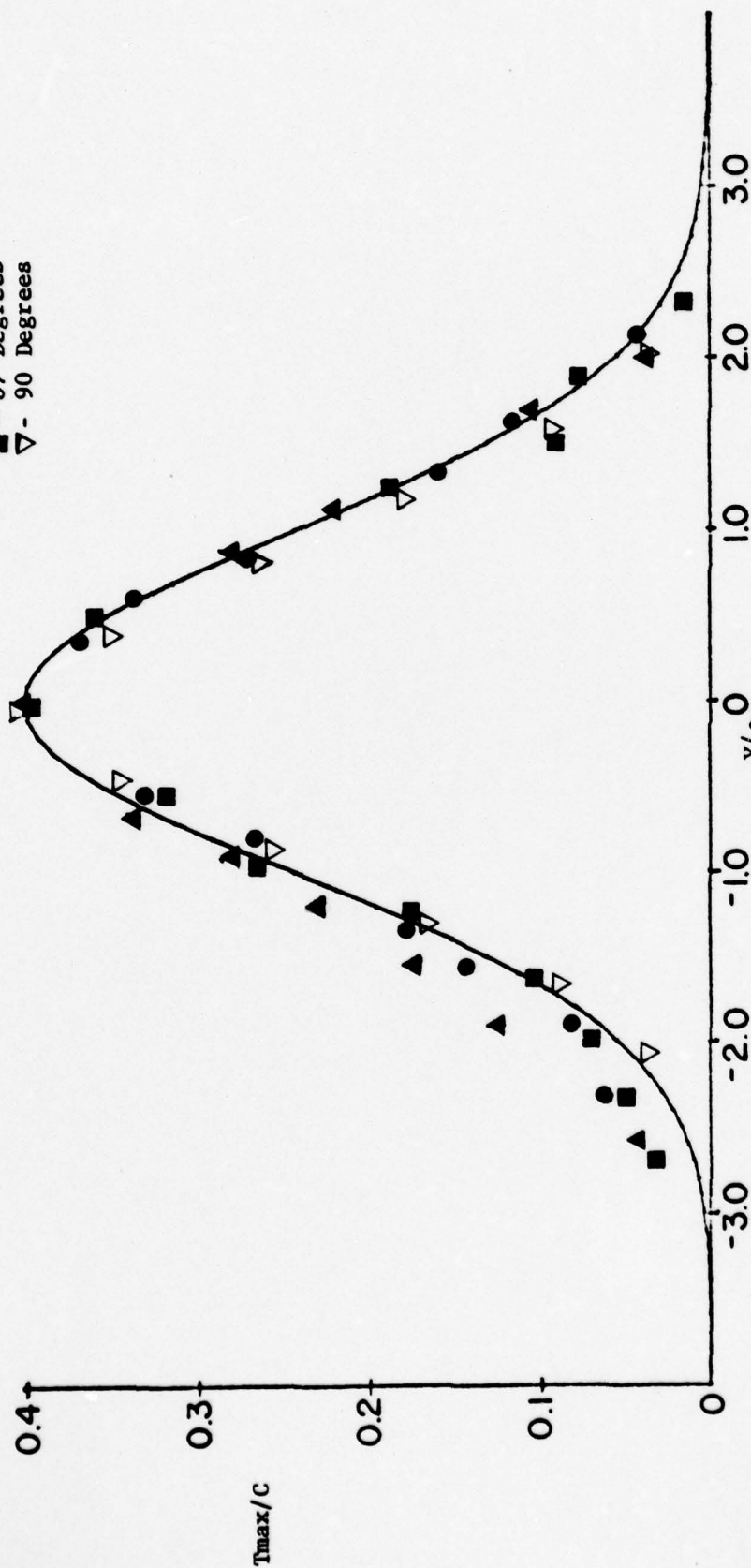Figure 28

Comparison of Horizontal Distribution of Temperature to a
Standard Normal Distribution for Angles of Incidence at
25.8 Jet Diameters Downwind from the Nozzle

73

Figure 29

Comparison of Horizontal Distribution of Temperature to a
Standard Normal Distribution for Angles of Incidence at
34.5 Jet Diameteres from the Nozzle

Angles of Incidence

▲ - 29 Degrees
● - 45 Degrees
■ - 67 Degrees

Tmax/C

Y/Q

74

Angles of Incidence

▲ - 29 Degrees
● - 45 Degrees
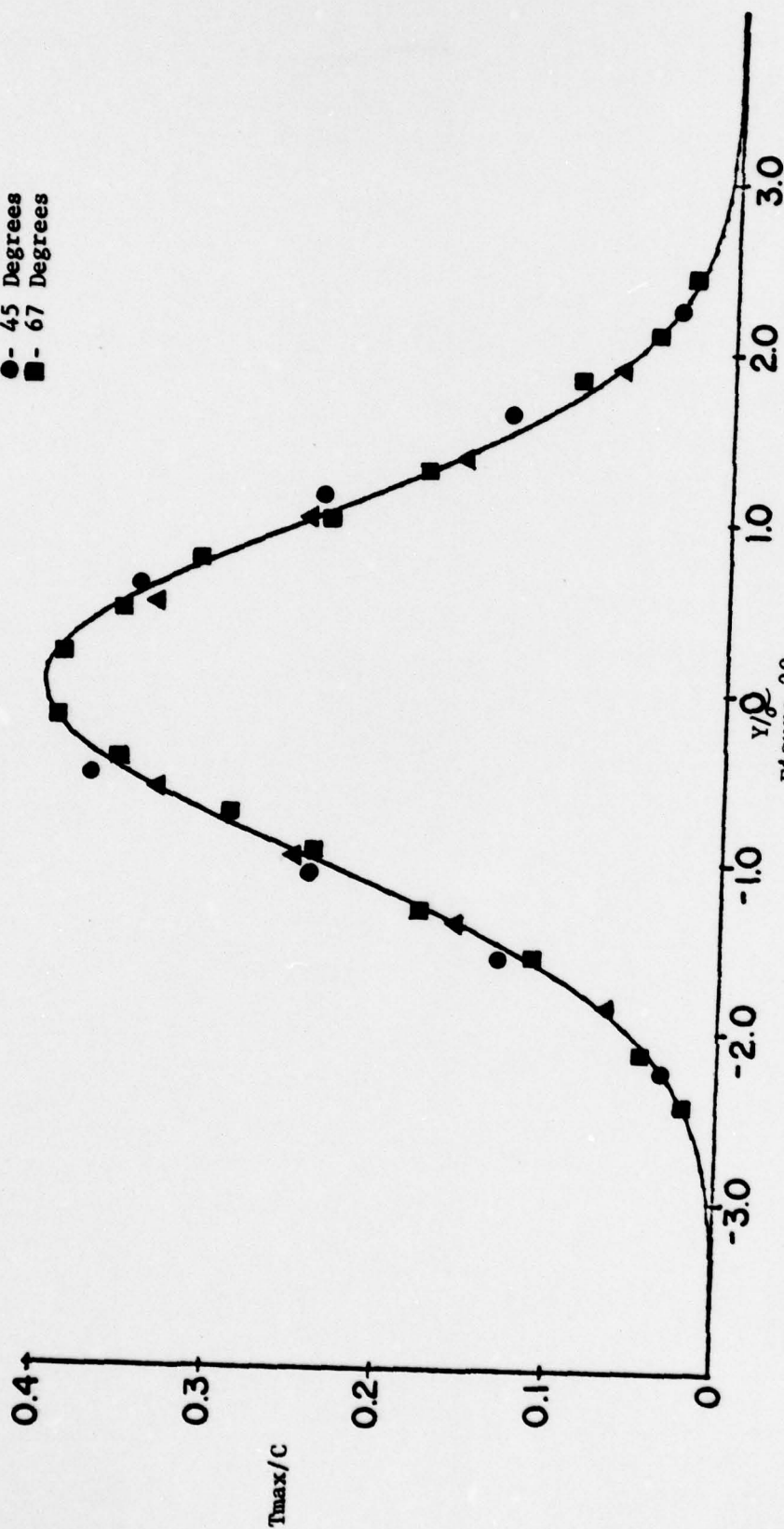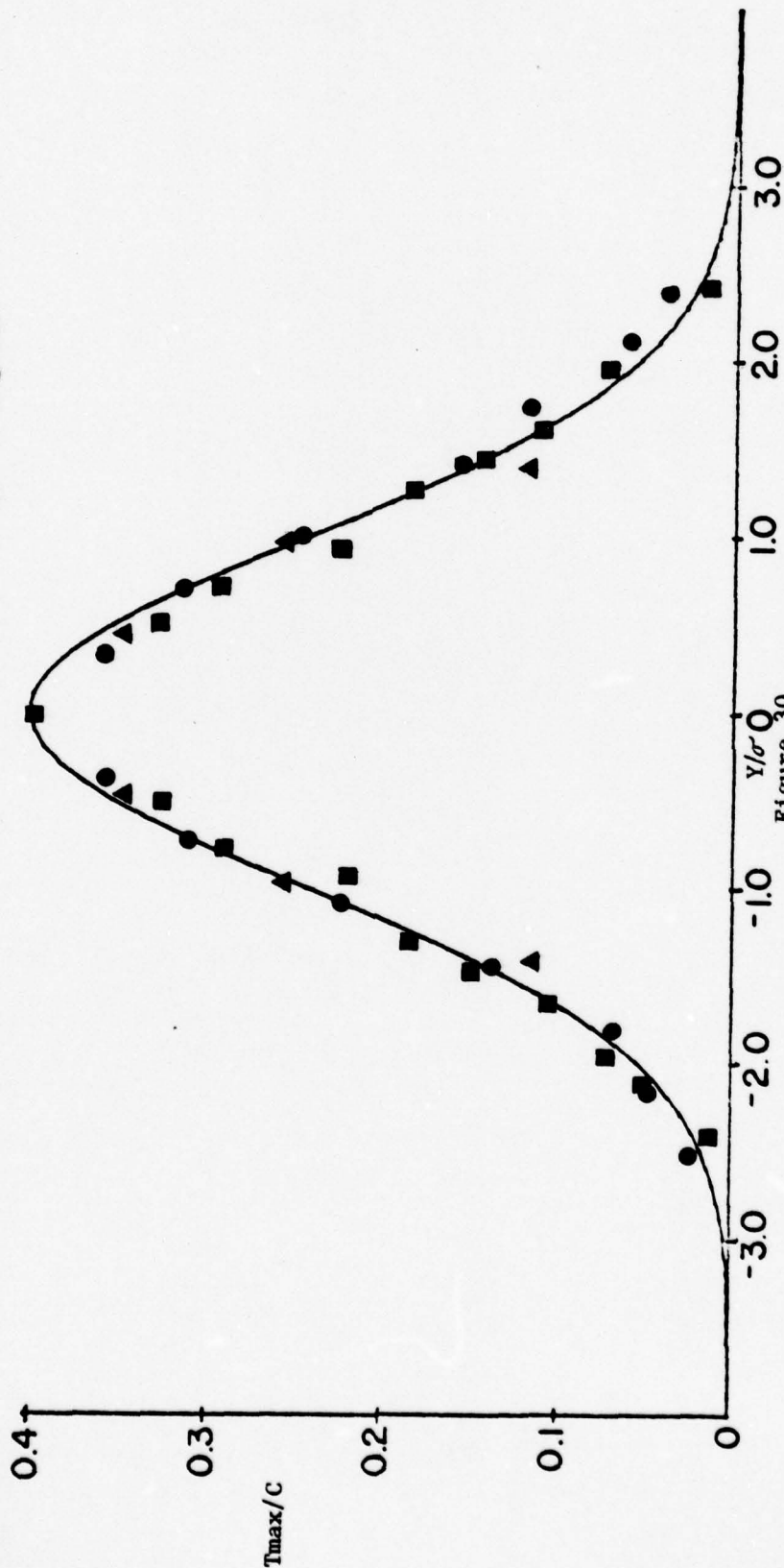■ - 67 Degrees

T_{max}/C

Y/σ

Figure 30

Comparison of Horizontal Distribution of Temperature to a
Standard Normal Distribution for Angles of Incidence at
51.7 Jet Diameters from the Nozzle

Figure 31

Comparison of Horizontal Distribution of Temperature to a
Standard Normal Distribution for Angles of Incidence at
86.2 Jet Diameters Downwind from the Nozzle

Angles of Incidence

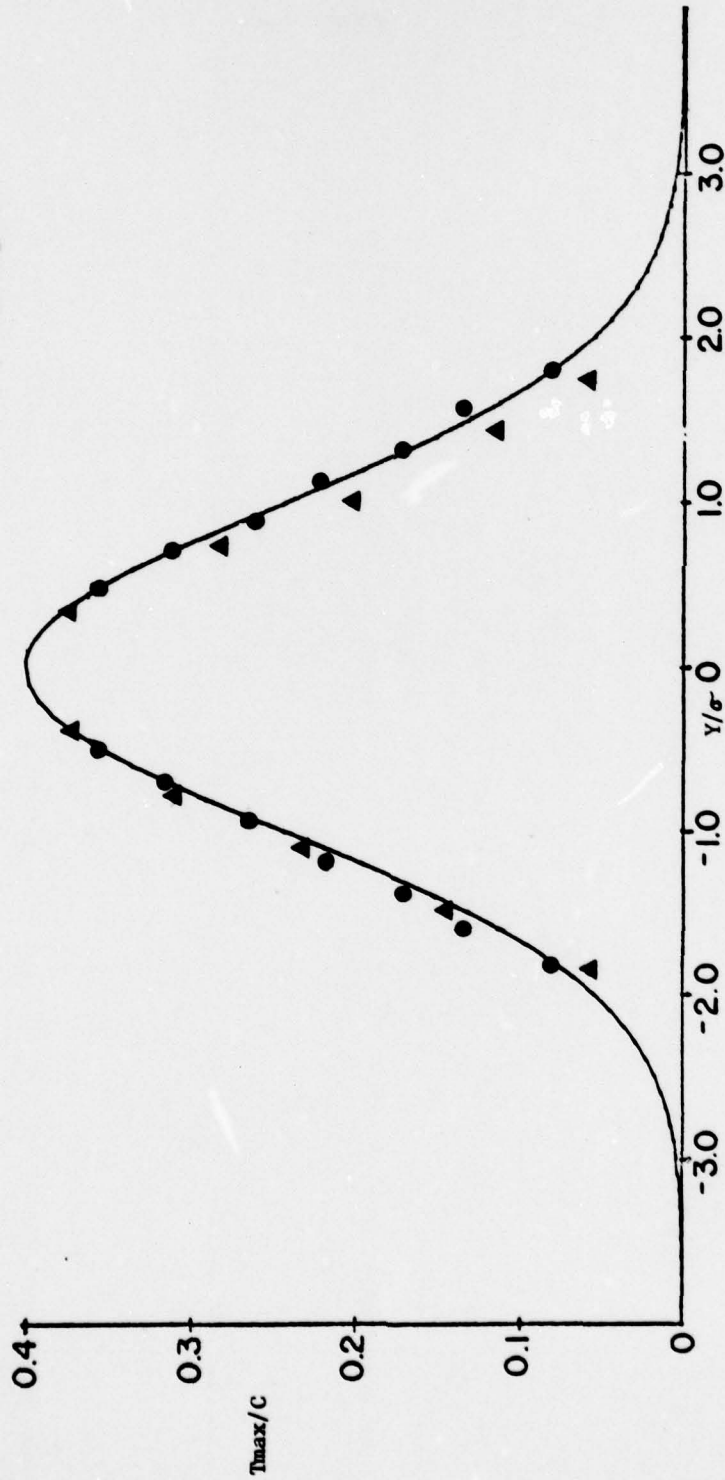▲ - 29 Degrees
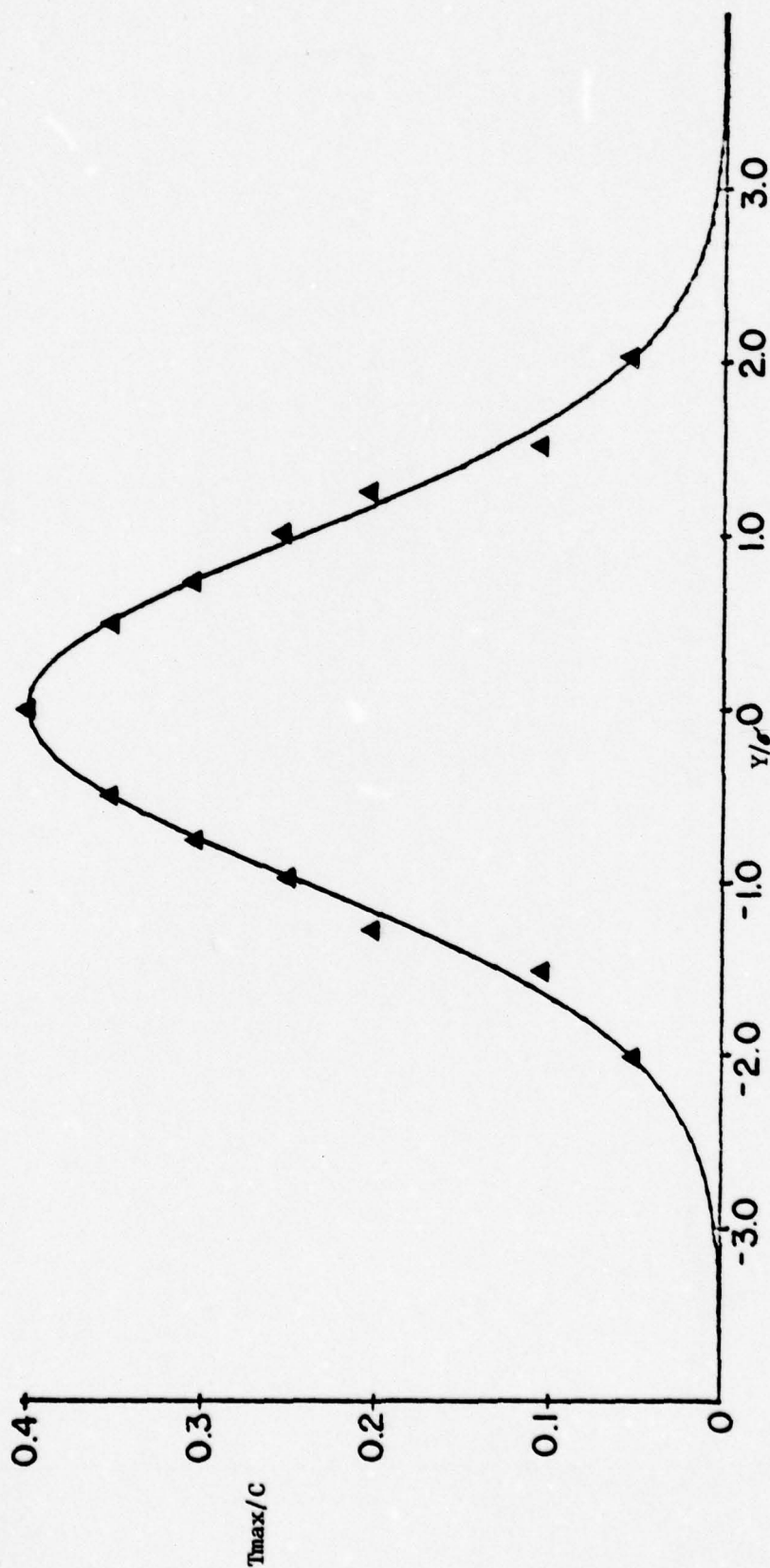
Figure 32

Comparison of Horizontal Distribution of Temperature to a
Standard Normal Distribution for Angles of Incidence at
120.6 Jet Diameters Downwind from the Nozzle

77
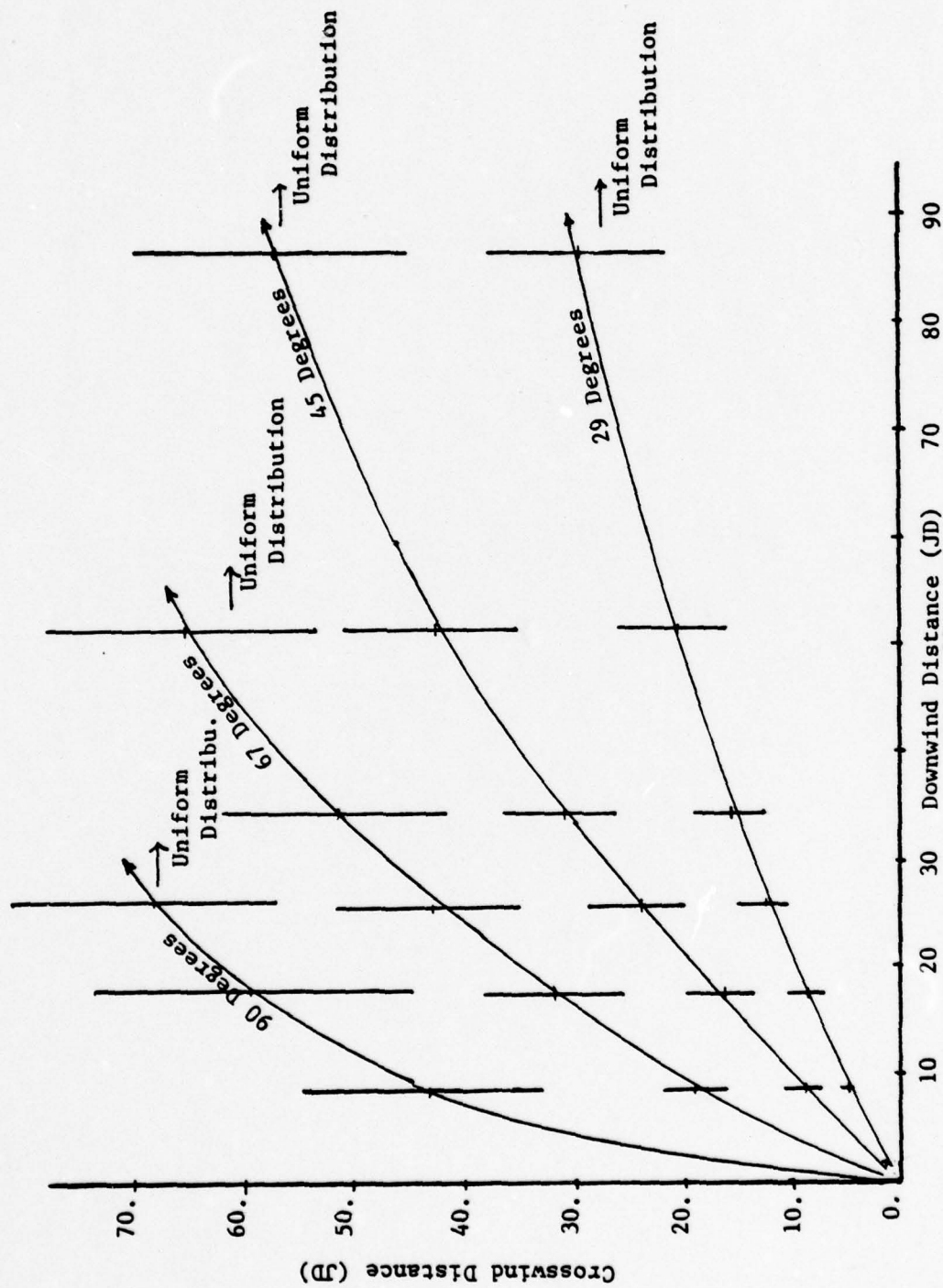
Spatial Representation of Plume Width as a Function of
Downwind and Horizontal Distances from the end of the
Nozzle for Different Angles of Incidence to the Wind

Figure 33

78
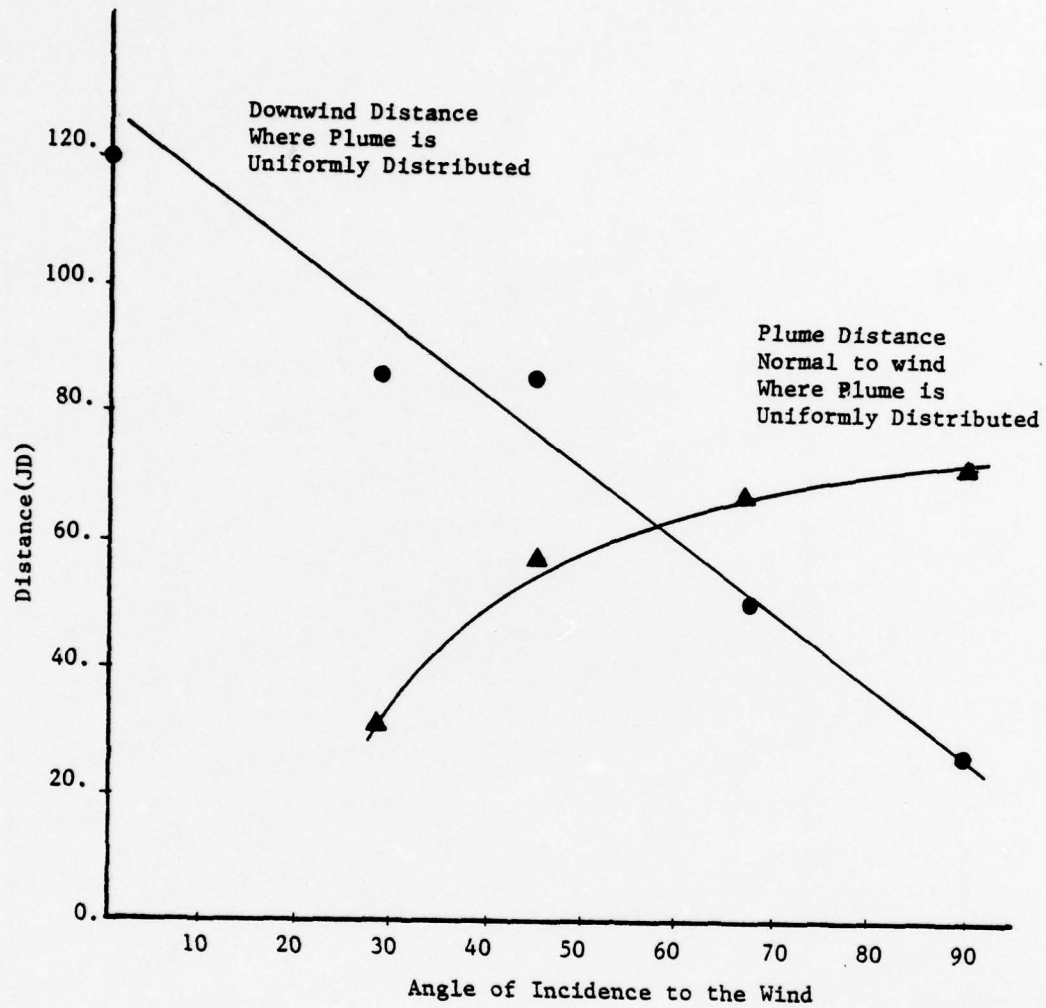
Figure 34

Distance Downwind and Normal to Wind from the Nozzle
Where the Plume is Uniformly Distributed
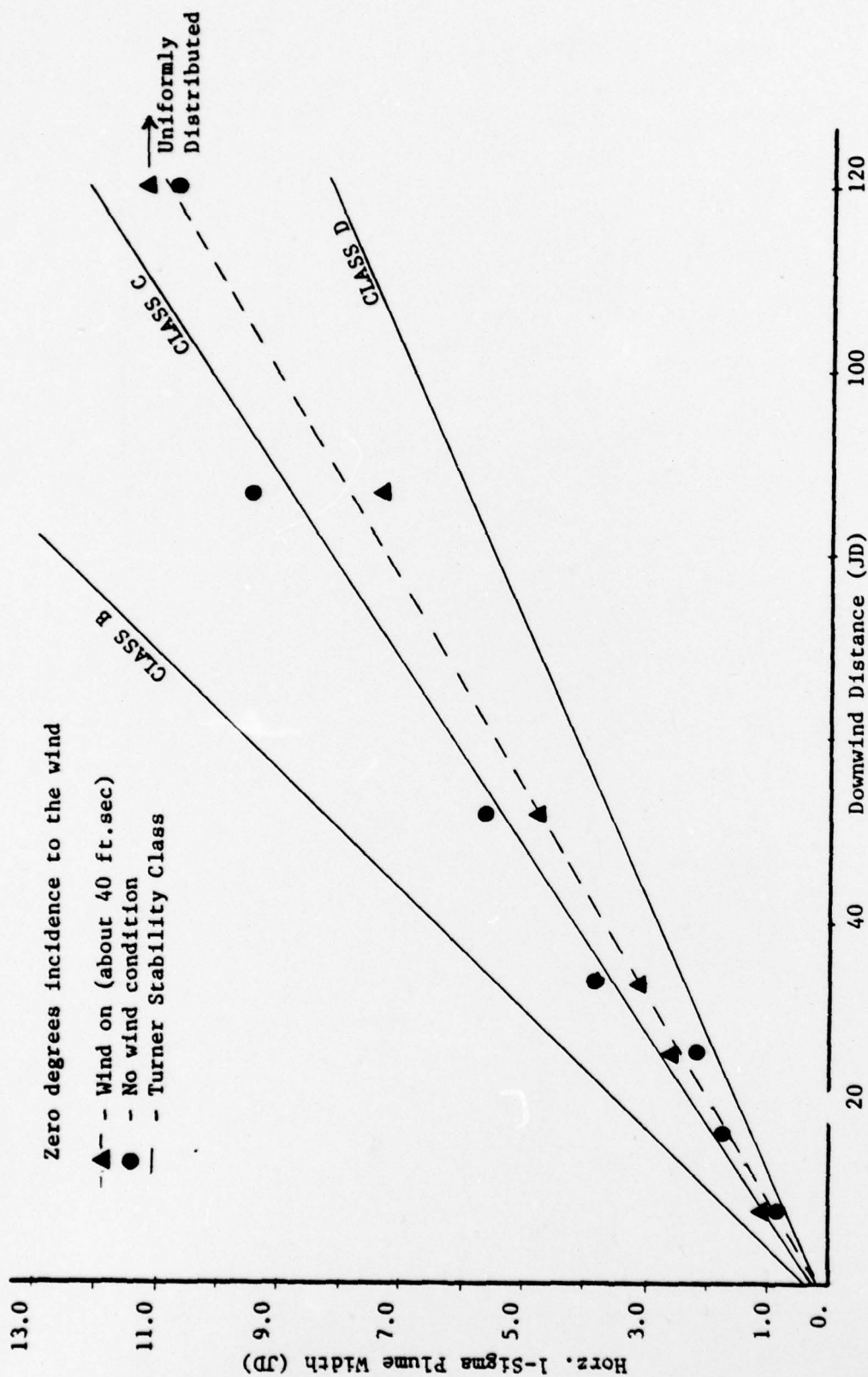
Figure 35

Horizontal Plume Width vs. Downwind Distance

80
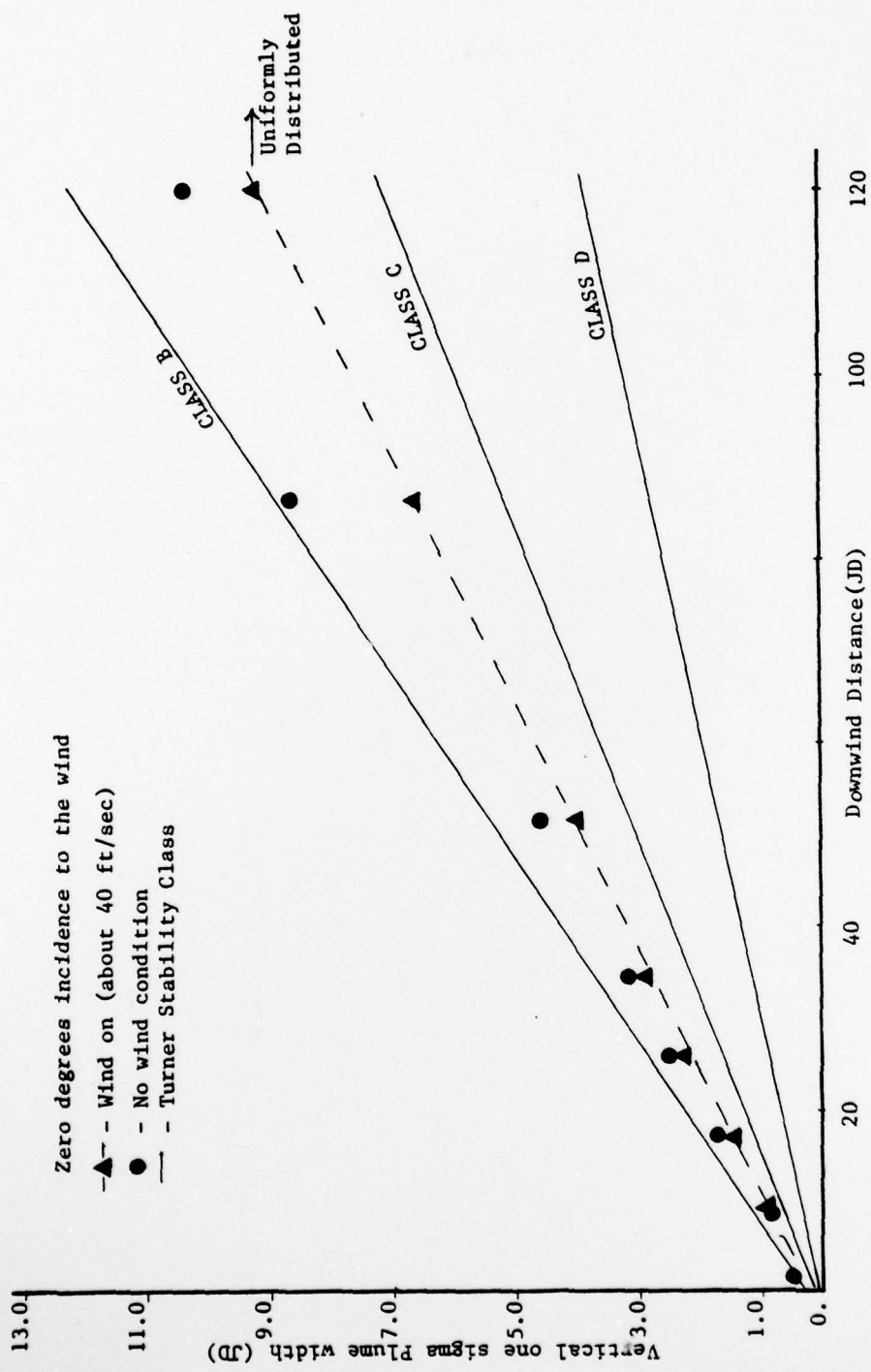
Figure 36

Vertical Plume Width vs. Downwind Distance
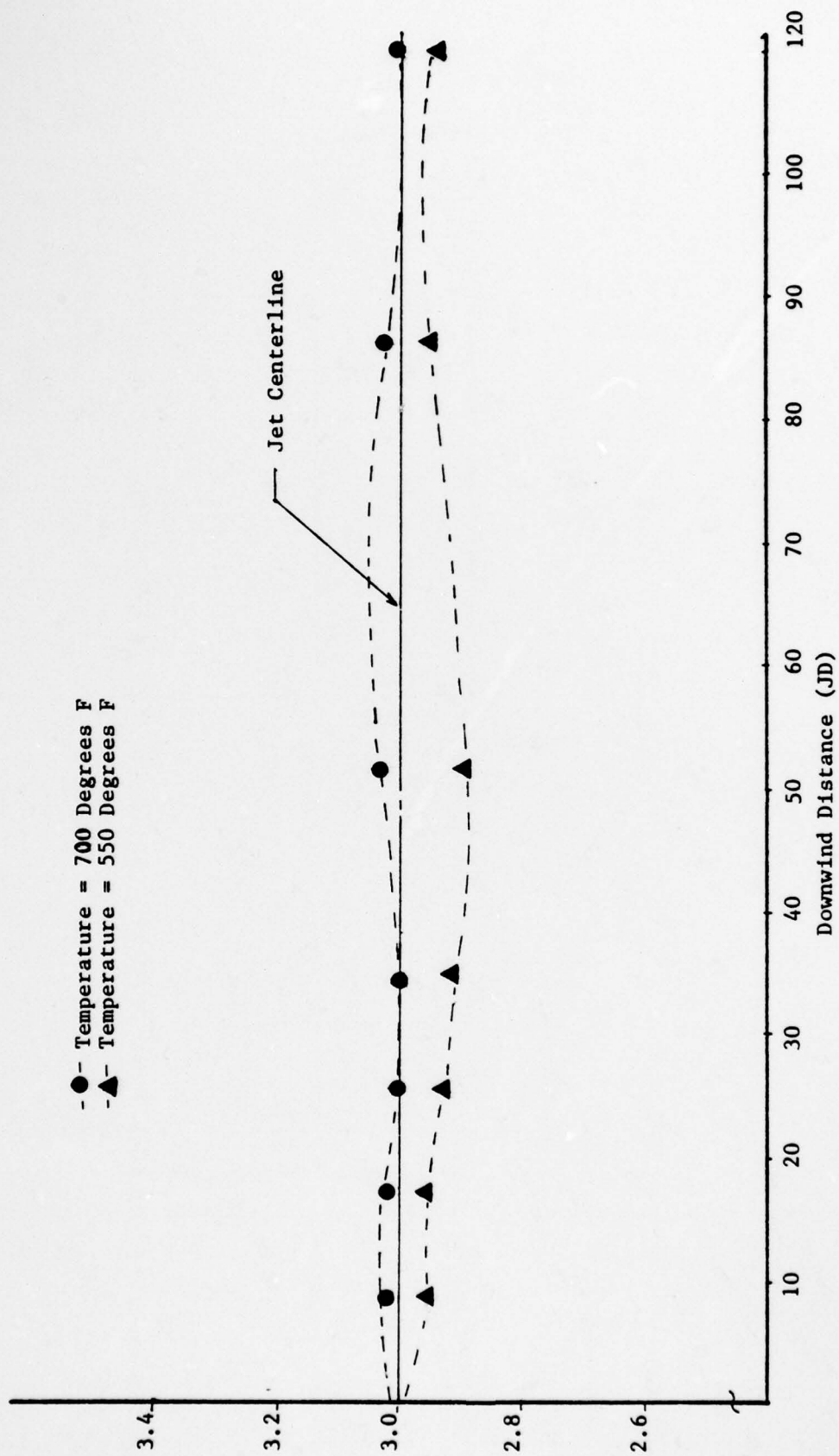
Plume Rise vs. Downwind Distance

Figure 37

82
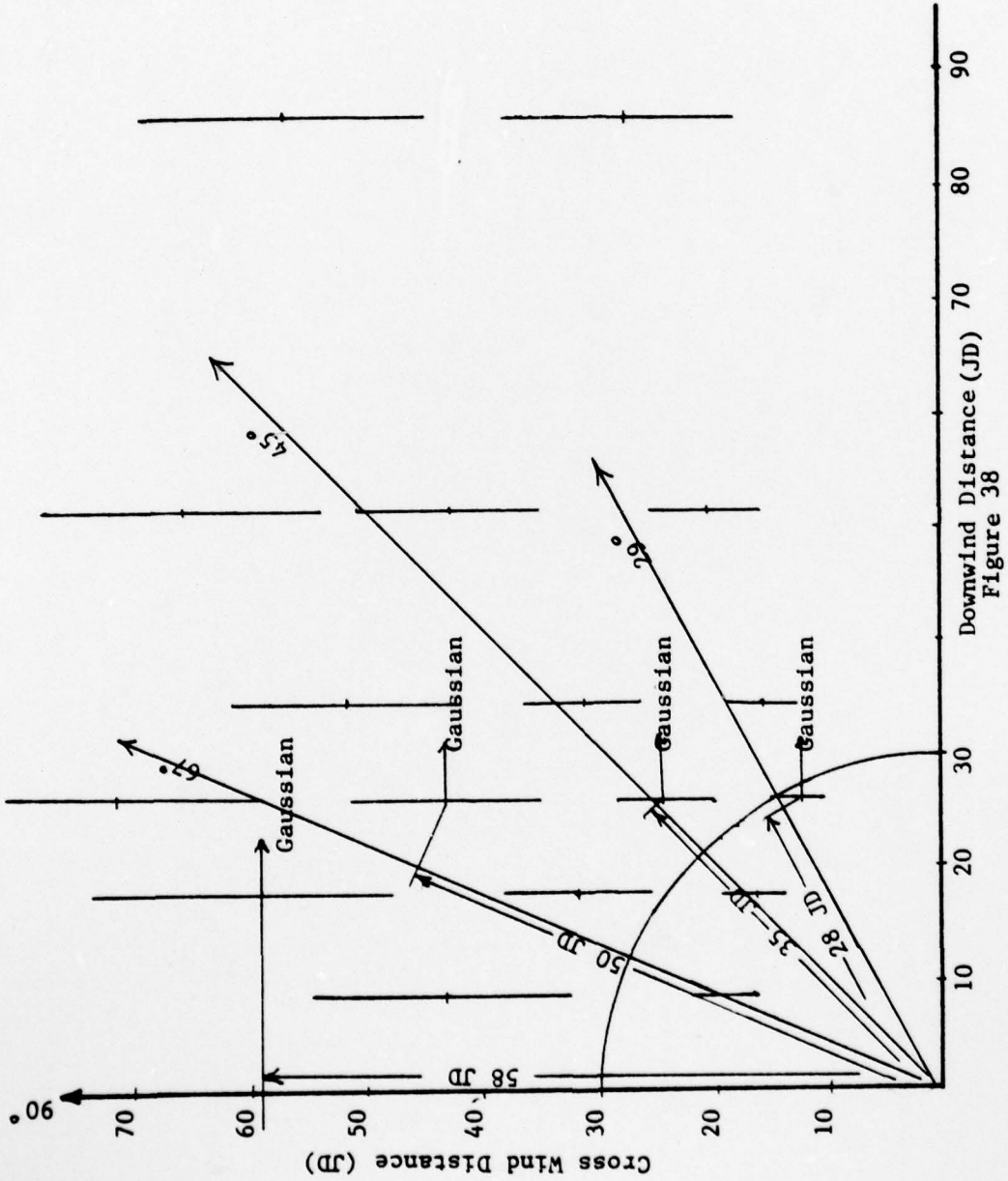
Jet Penetration vs. Downwind and Horizontal Distance from
the Nozzle for Different Angles of Incidence to the Wind

Downwind Distance (JD) 70
Figure 38

Figure 39

Jet Penetration Distance along the Jet
Axis vs. Angle of Incidence
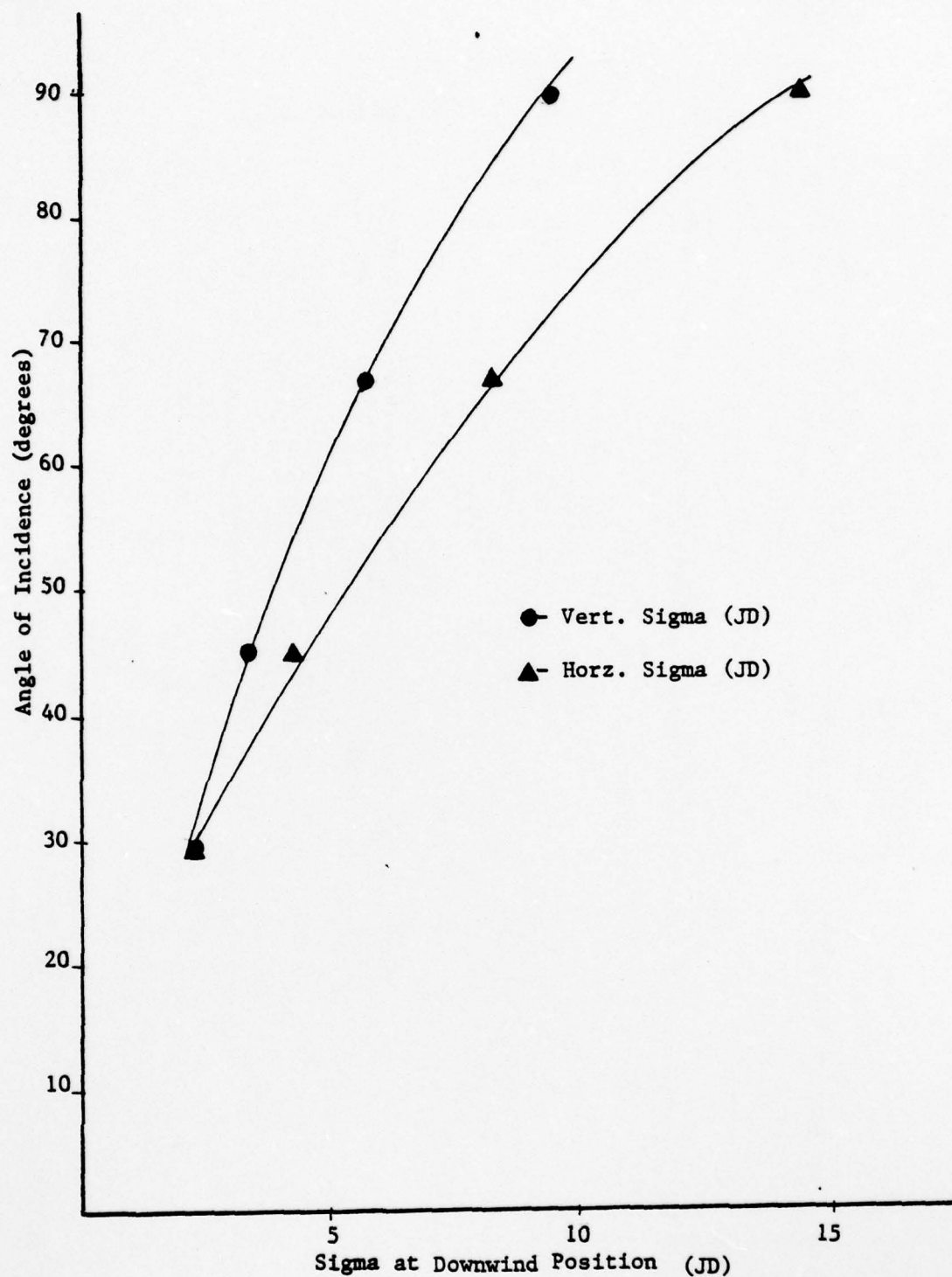
Figure 40
1-Sigma Width of Plume At Gaussian Position
vs. Angle of Incidence to the Wind

σ's Vertical (JD)

σ's Horizontal (JD)

| Downwind Distance (JD)	wind off choked	wind on			wind off choked	wind on		
		choked	unchoked	hi-temp		choked	unchoked	hi-temp
1.72	.574	.574	.862	-	.862	.862	1.0	-
8.62	.862	.862	.862	.862	.862	1.25	1.0	1.0
17.3	1.72	1.44	1.72	2.01	1.72	1.72	2.16	2.16
25.8	2.44	2.29	2.44	2.29	2.16	2.58	2.80	2.70
34.5	3.16	2.90	3.16	3.16	3.87	3.02	3.50	3.40
51.7	4.59	4.02	4.31	4.31	5.60	4.74	5.28	5.30
86.2	8.62	6.61	8.04	6.90	9.48	7.32	8.01	7.75
120.6	10.34	9.19	9.77	10.34	10.7	11.2	11.2	11.0

TABLE I

1-Sigma Plume Width of the Vertical and Horizontal
Temperature Profiles at Zero Degrees Incidence
to the Wind as a Function of Downwind
Distance for Different Nozzle Conditions

	Sigma Vert. (JD) (choked) Blockage				Sigma Horz. (JD) (choked) Blockage		
	none	small	large		none	small	large
1.72	.574	.574	.574		.862	.862	.862
8.62	1.00	1.00	1.00		.862	.862	1.29
17.3	1.43	1.43	1.72		1.72	1.72	1.72
25.8	2.30	2.30	2.30		2.58	2.60	3.01
34.5	2.90	3.16	3.44		3.01	3.00	3.87
51.7	4.02	4.59	4.59		4.74	4.90	5.17
86.2	6.61	7.04	7.75		7.32	7.50	7.75
120.6	9.19	.19	9.19		11.20	11.30	10.34

Downwind Distance JD

Table II

1-Sigma Plume Width of the Vertical and Horizontal
Temperature Profiles at Zero Degrees
Incidence to the Wind for Different
Nozzle Blockages

87

Downwind Distance (JD)	Sigma Vert. (JD)					Sigma Horz. (JD)				
	0°	29°	45°	67°	90°	0°	29°	45°	67°	90°
1.72	.574	.574	–	–	4.31	.862	.287	.574	2.01	11.49
8.62	.862	.862	1.15	2.29	6.03	1.25	.862	1.44	2.87	11.49
17.3	1.44	1.72	2.29	4.31	9.54	1.72	1.72	3.16	6.32	14.36
25.8	2.29	2.44	3.45	5.75	–	2.58	2.29	4.31	8.33	14.36
34.5	2.90	3.16	4.59	7.47	–	3.02	3.45	5.17	10.15	–
51.7	4.02	4.89	6.89	11.49	–	4.74	5.17	8.04	12.06	–
86.2	6.61	8.62	10.91	–	–	7.32	8.04	12.64	–	–
120.6	9.19	12.64	–	–	–	11.20	11.49	–	–	–

Table III

1-Sigma Plume Width of the Vertical and Horizontal
Temperature Profiles for Different Angles of
Incidence to the Wind

IV. SUMMARY AND RECOMMENDATIONS

In summary, a neutrally stable atmospheric surface layer was suitably simulated in a low speed wind tunnel. Horizontal and vertical temperature profiles aft of a nozzle which was immersed in that flow were measured. The dispersion data from the simulated jet exhaust were evaluated for different nozzle conditions and compared to the dispersion data used in the AQAM Model.

It is recommended that additional studies be made for conditions of other than neutral stability. Measurements made in less stable surface layers would provide a better understanding of the plume rise and looping phenomenon. These data should further enhance the predicting capability of AQAM.

LIST OF REFERENCES

1. Air Force Weapons Laboratory Report AFWL-TR-74-304
    A Generalized Air Quality Assessment Model for
    Air Force Operations, by D. M. Rote and
    L. E. Wangen, February 1975

2. Air Force Weapons Laboratory Report AFWL-TR-74-54
    A generalized Air Quality Assessment Model for
    Air Force Operations--An Operators Guide, by
    D. M. Rote and L. E. Wangen, June 1974

3. Civil and Environmental Engineering Development
    Office (Air Force Systems Command)
    Report CEEDO-TR-76-34,
    Air Quality Assessment Model for Air Force Operations
    Short Term Emission/Dispersion Computer Code
    Documentation, by D. J. Bingaman, April 1977

4. Naval Postgraduate School Report
    NPS-57Nt-75071A, Modification of An
    Ambient Air Quality Model for Assessment
    of U.S. Naval Aviation Emittants,
    by K. I. Weal and D. W. Netzer, August 1975

5. Naval Postgraduate School Report
    NPS-67Nt76091, An Ambient Air Quality Model
    for Assessment of U.S. Naval Aviation Emittants,
    by G. Thompson and D. W. Netzer, September 1976

6. Civil and Environmental Engineering Development
    Office (Air Force Systems Command)
    Report CEEDO-TR-77-57,
    Photographic Measurements of USAF Aircraft Plume Rise,
    by P. D. Music, J. S. Hunt, and D. F. Naugle,
    November 1977

7. Cornell Aeronautical Laboratory, Inc. Report
    VC-2740-5-1, On the Laboratory Simulation of Small
    Scale Atmospheric Turbulence, by T. R. Sundaram
    and G. R. Ludwig, December 1969

8. Sundaram T. R., Ludwig G. R., and Skinner C. T.,
    "Modeling of the Turbulence Structure of the
    Atmospheric Surface Layer", AIAA Journal
    Vol.10, No. 6, p. ?43-750, June 1972

9. Cermak, J. E. "Laboratory Simulation of the
    Atmospheric Boundry Layer", AIAA Journal
    Vol. 9, No. 9, p. 1746-1753, September 1971

10. Cermak J. E., <u>Applications of Fluid Mechanics</u>
    <u>to Wind Engineering, A Freeman Scholar Lecture,</u>
    paper presented at the Winter Annual Meeting
    of the American Society of Mechanical Engineers,
    New York, N.Y., 17-21 November 1974

11. Fluid Mechanics Program, Engineering Research
    Center College of Engineering, Colorado State
    University, Project THEMIS Report TR-17,
    <u>Wind Tunnel Modeling of Flow and Diffusion</u>
    <u>Over an Urban Complex,</u> by F. H. Chaudhry
    and J. E. Cermak, May 1971

12. Fluid Mechanics Program, Engineering Research
    Center College of Engineering, Colorado State
    University, Project THEMIS Report TR-11,
    <u>An Investigation of Flow Over High Roughness</u>,
    by, T. Kawatani and W. Z. Sadeh, August 1971

13. Fluid Mechanics Program, Engineering Research
    Center College of Engineering, Colorado State
    University, Project THEMIS Report TR-12,
    <u>Numerical Similation of Wind, Temperature,</u>
    <u>Shear Stress, and Turbulent Energy Over</u>
    <u>Non-Homogeneous Terrain,</u> by Chin-hua Huang
    and E. C. Nickerson, p. 21-28, March 1972

14. Monin, A. S. and Obukhov A. M., "Basic Regularity
    in Turbulent Mixing in the Surface Layer of the
    Atmosphere", <u>USSR Acad. Sci. Works of Geophysics</u>
    <u>Met.,</u> N0. 24 p. 163, 1954

15. Schlichting, H., <u>Boundary Layer Control,</u>
    McGraw Hill, 1955

16. Turner, D. B., "Workbook of Atmospheric
Dispersion Extimates", U.S. Dept. of Health,
Education, and Welfare, U.S. Public Health Service
Publication NØ. 999-AP-26, January 1974

INITIAL DISTRIBUTION LIST